NASA TM–20250002085

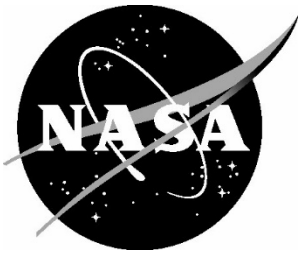

Documentation for Goddard Ocean Tide Solution GOT5: Global Tides from Multi-mission Satellite Altimetry

Richard D. Ray
Goddard Space Flight Center, Greenbelt, Maryland

February 2025

NASA STI Program Report Series

Since its founding, NASA has been dedicated to the advancement of aeronautics and space science. The NASA scientific and technical information (STI) program plays a key part in helping NASA maintain this important role.

The NASA STI program operates under the auspices of the Agency Chief Information Officer. It collects, organizes, provides for archiving, and disseminates NASA's STI. The NASA STI program provides access to the NTRS Registered and its public interface, the NASA Technical Reports Server, thus providing one of the largest collections of aeronautical and space science STI in the world. Results are published in both non-NASA channels and by NASA in the NASA STI Report Series, which includes the following report types:

- TECHNICAL PUBLICATION. Reports of completed research or a major significant phase of research that present the results of NASA Programs and include extensive data or theoretical analysis. Includes compilations of significant scientific and technical data and information deemed to be of continuing reference value. NASA counterpart of peer-reviewed formal professional papers but has less stringent limitations on manuscript length and extent of graphic presentations.

- TECHNICAL MEMORANDUM. Scientific and technical findings that are preliminary or of specialized interest, e.g., quick release reports, working papers, and bibliographies that contain minimal annotation. Does not contain extensive analysis.

- CONTRACTOR REPORT. Scientific and technical findings by NASA-sponsored contractors and grantees.

- CONFERENCE PUBLICATION. Collected papers from scientific and technical conferences, symposia, seminars, or other meetings sponsored or co-sponsored by NASA.

- SPECIAL PUBLICATION. Scientific, technical, or historical information from NASA programs, projects, and missions, often concerned with subjects having substantial public interest.

- TECHNICAL TRANSLATION. English-language translations of foreign scientific and technical material pertinent to NASA's mission.

Specialized services also include organizing and publishing research results, distributing specialized research announcements and feeds, providing information desk and personal search support, and enabling data exchange services.

For more information about the NASA STI program, see the following:

- Access the NASA STI program home page at http://www.sti.nasa.gov

.

NASA TM–20250002085

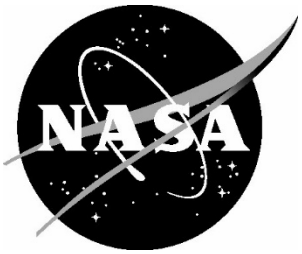

Documentation for Goddard Ocean Tide Solution GOT5: Global Tides from Multi-mission Satellite Altimetry

Richard D. Ray
Goddard Space Flight Center, Greenbelt, Maryland

National Aeronautics and
Space Administration

Goddard Space Flight Center
Greenbelt, Maryland

February 2025

Available from:

NASA STI Program / Mail Stop 050
NASA Langley Research Center
Hampton, VA 23681-2199

Summary

Goddard Ocean Tide GOT5 is a new solution for the amplitudes and phases of the daily and sub-daily global ocean tides, based on decades of radar altimetry from multiple satellite missions. Over the main part of the deep ocean, between latitudes ±66°, the solution rests primarily with the series of five satellites Topex/Poseidon, Jason-1, Jason-2, Jason-3, and Sentinel-6A Michael Freilich, but in shallow seas and in polar latitudes other satellite altimeters were also used. The tidal analysis of these data was done relative to a prior model, which for the most part was the Finite Element Solution FES2014 of Lyard et al. (2021), with some minor patches. The GOT5 solutions were thus starting with a very good global model, and the obtained results benefit greatly from that. This report documents some of the data processing details underlying the GOT5 tides. There are several variants of GOT5, arising not only from (experimental) refinements in processing algorithms but also from different approaches to handling the problem of atmospheric loading; a special variant, GOT5.5D, was designed to be used in conjunction with the current version of the Dynamic Atmosphere Correction by attempting to overcome inadequacies in adopted models of atmospheric tides. This report includes a comprehensive set of cotidal charts for twenty constituents in the diurnal, semidiurnal, terdiurnal, and quarter-diurnal bands.

Acknowledgments: I thank my colleagues within the Geodesy & Geophysics Laboratory at GSFC for many years of helpful discussions on all aspects of satellite altimetry. In particular I am indebted to Brian Beckley for his help and for his ever-improving altimeter datasets and to Frank Lemoine for commenting on the whole report. I also thank Ole Andersen and his colleagues for releasing their invaluable retracked CryoSat-2 data over polar oceans. The RADS altimeter database, now mostly maintained by Remko Scharroo (Eumetsat) and Eric Leuliette (NOAA), was also heavily employed in this work. It is a pleasure to acknowledge many discussions with Florent Lyard (CNRS) and Loren Carrère (CLS), who led the development of the FES2014 model that was heavily exploited in this work. Loren Carrère and Perrine Abjean also kindly helped with the analysis of ECMWF air tides by computing the results shown in Figure 16b.

All figures in this document were created with the GMT plotting package, written by the late Paul Wessel (University of Hawaii) and Walter Smith (NOAA) and subsequently upgraded and supported by them and others. The document was typeset with the LaTeX system.

Contents

1 Introduction

This report documents a global ocean tide atlas created by tidal analysis of decades of radar altimeter data collected from multiple satellite missions. It thus continues a series of works that use longer and longer time series and often-reprocessed datasets of altimetry, plus ever-improving methods of analysis, to achieve more accurate mapping of global ocean tides. In many respects, the approach here follows that laid out with my colleague Ernst Schrama in the early 1990s (E. J. O. Schrama & Ray, 1994; Ray, 1999). It uses a "binning" approach to tidal analysis of altimetry, allowing quasi-localized solutions, and it employs a "remove-restore" method, thereby providing corrections to an adopted prior tide model. Many details of the analysis have been refined over time. Moreover, the advances in accuracy also benefit from ever-improving prior models. Although a series of different prior models, including some local or regional tide models, have been used over time in the development of GOT models, most—including the main prior used here—have benefited immeasurably from work done in France, first by the late Christian Le Provost's group in Grenoble and then later by Florent Lyard's group in Toulouse (Le Provost et al., 1994; Lyard et al., 2006, 2021).

The new altimeter solution described in this report, dubbed GOT5, has several variants at the time of writing: GOT5.1, GOT5.5, GOT5.5D, and GOT5.6. The first three differ primarily in how atmospheric loading (inverted barometer, etc.) was handled. GOT5.1 was not released, as it had some clear inadequacies in polar regions, but it has been used for processing some altimeter data at GSFC (B. Beckley, pers. comm.) and it is referred to in places below. GOT5.5D is a experimental version of GOT5.5 to be used only in conjunction with the current version of Dynamic Atmosphere Correction (DAC), a correction for atmospheric loading that is widely applied by altimeter users. The need for this unusual complication is explained in Section 5.3. As will be seen, the problem it addresses is only partially solved by having a separate tide model. GOT5.6 is the same as 5.5, but with the addition of four small constituents arising from the third-degree terms in the astronomical potential (Ray, 2020). Aside from these constituents, GOT5.5 is equivalent to GOT5.6. All solutions sit on a (1/8)° global grid.

The GOT5 constituents cover the diurnal and semidiurnal tidal bands, plus one terdiurnal and two quarter-diurnal waves. It does not include long-period constituents. For these, I can still recommend using some hydrodynamic solutions produced with my colleague Lana Erofeeva and described in Ray & Erofeeva (2014). The tar file for that model also includes a self-consistent equilibrium solution for the 18.6-year node tide.

As of this writing, the GOT5 (and also Ray-Erofeeva long-period) tides can be obtained via the GSFC website `https://earth.gsfc.nasa.gov/geo/data/ocean-tide-models`. Government data-distribution policies change often, however, so that link is unlikely to last.

In the near future there may be minor updates to GOT5, arising from improvements in certain areas or from better handling of the DAC (see below). However, the next major upgrade (e.g., GOT6) will occur as we begin incorporating tidal solutions from SWOT, which has the potential to greatly improve the mapping of near-coastal tides (Hart-Davis et al., 2024).

2 Constituent Selection

As the altimeter time series gets ever longer, it allows us to incorporate a more complete tidal spectrum into the solutions. The FES2014 atlas (Lyard et al., 2021) entails 34 constituents, as does the new FES2022. It is important to realize that even when past models typically provided only 8 or so main constituents, many more were accounted for by the tide prediction software distributed with the models (e.g., see Section 8), usually by automatic inference. For example, GOT4 was released with ten constituents, but its associated tide-prediction software returned tidal elevations based on 26 constituents plus any necessary lunar nodal and/or perigee side-lines.

GOT5.5 includes global solutions for 16 short-period constituents. GOT5.6 supplements this with four additional solutions for third-degree constituents, although they are confined to the latitude band ±66°.[1] Table 1 lists these tides. The distributed GOT5.5 tar file also includes 17 minor constituents that have been inferred from the primary constituents; these are unneeded for tide prediction by the `perth5` software (Section 8) but they are included as a convenience to users with other applications (e.g., the GSFC GEODYN orbit determination software requires some of these minor constituents be entered explicitly). For any inferred constituents in the diurnal band, the resonance effect from the earth's fluid core has been accounted for (Ray, 2017). The inferred constituents are:

$$2Q_1,\ \chi_1,\ \tau_1,\ \rho_1,\ M_1,\ \pi_1,\ \psi_1,\ \phi_1,\ \theta_1,\ SO_1,\ \varepsilon_2,\ \nu_2,\ L_2,\ \lambda_2,\ T_2,\ R_2,\ \eta_2.$$

As Table 1 indicates, GOT5 includes two quarter-diurnal tides. In retrospect, and after testing these tides (see Section 7), I probably should have included at least MN_4 and perhaps a few other compound tides, since altimetry is now evidently capable of recovering these to some extent, even without benefit of SWOT data.

Whether a particular constituent should be included explicitly in the solution or instead computed by inference depends on (1) the sampling characteristics of the satellite, (2) general noise levels, (3) whether a constituent is perturbed by nonlinear effects, and/or (4) whether the constituent sits at the edge of a tidal frequency band, which would necessitate extrapolation rather than interpolation of admittances (see related discussion by M. G. Hart-Davis, Dettmering, et al., 2021). As the altimeter series lengthens, noise levels reduce, and more constituents can be determined directly. For example, in earlier GOT tide solutions it was generally found that P_1 was more accurate if inferred from K_1; with the current altimeter time series, this is (mostly) no longer the case.

For small constituents like ν_2, M_1, ρ_1, etc., inference is still probably more accurate everywhere than direct estimation. In contrast, the constituents σ_1, J_1, and OO_1 are at the edges of the diurnal band where admittance extrapolation is risky, so these tides in GOT5 were determined directly (see again the discussion of trade-offs by M. G. Hart-Davis, Dettmering, et al. (2021)). Tides σ_1 and $2Q_1$, separated by 2 cpy in frequency, have comparable amplitudes, although the former is slightly larger in the astronomical potential, and thus I selected σ_1 for direct estimation and allowed $2Q_1$ to be later inferred from σ_1 and Q_1.

The case of μ_2 falls under category (2)—it is often perturbed in shallow water by the nonlinear compound tide $2MS_2$, occurring at exactly the same frequency. But the perturbation can also be

[1]The reason why the four degree-3 tides were not simply included in GOT5.5 is because I had promised certain project software planners that GOT5 would have only 16 constituents. As their anticipated software would be fixed to these 16, they could still use model GOT5.5, but others could incorporate the degree-3 tides by moving to GOT5.6.

Table 1: Constituents explicitly included in GOT5

Constituent	Doodson no.	Frequency (°/h)
GOT5.5		
σ_1	127.5553	12.927140
Q_1	135.6553	13.398661
O_1	145.5553	13.943036
P_1	163.5553	14.958931
S_1	164.5552	15.000000
K_1	165.5551	15.041069
J_1	175.4551	15.585443
OO_1	185.5551	16.139102
$2N_2$	235.7550	27.895355
μ_2	237.5550	27.968208
N_2	245.6550	28.439730
M_2	255.5550	28.984104
S_2	273.5550	30.000000
K_2	275.5550	30.082137
M_4	455.5550	57.968208
MS_4	473.5550	58.984104
added in GOT5.6		
$^3M_1$	155.5552	14.492052
$^3N_2$	245.5551	28.435088
$^3L_2$	265.5553	29.533121
M_3	355.5552	43.476156

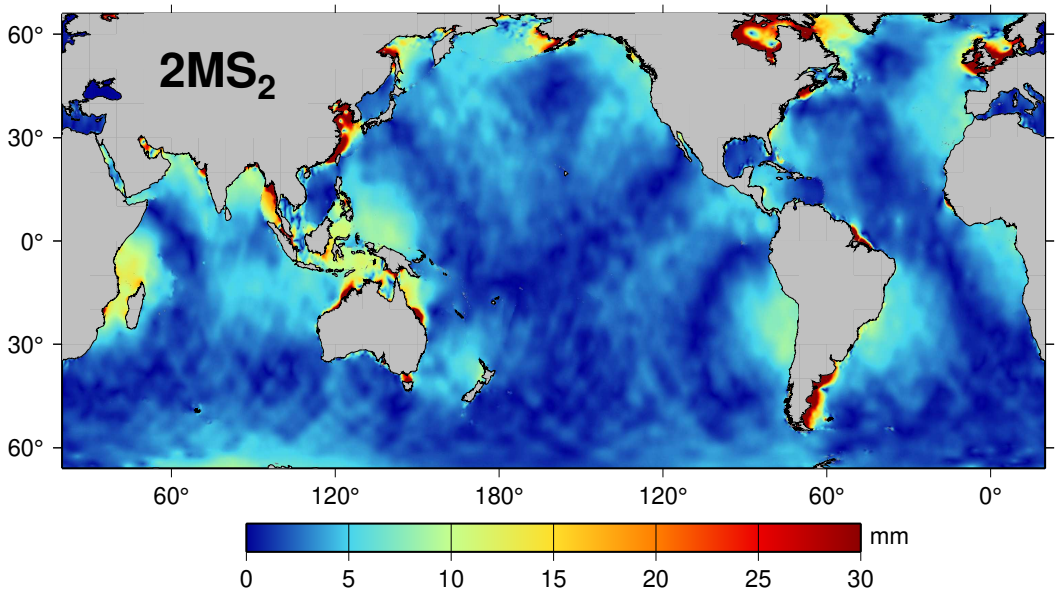

Figure 1: Amplitude of the compound tide $2MS_2$ as determined by subtracting the directly estimated μ_2 constituent from μ_2 as inferred from nearby constituents $2N_2$ and N_2. Although largest in shallow seas where it is generated by nonlinear frictional effects, $2MS_2$ is not totally confined to shallow water. This shows the importance of including μ_2 among the list of GOT5 constituents directly estimated from altimetry, as this nonlinear $2MS_2$ signal would be otherwise overlooked in GOT5 tide prediction.

detected in the deep ocean, as $2MS_2$ can evidently propagate from shallow water into deeper water, much as M_4 is known to do (Ray, 2007). In fact, even in the observed tidal admittance at Honolulu, presented by Munk & Cartwright (1966) as a classic case of smooth admittances that justified development of their response method, one notices that the admittance at μ_2 is slightly offset from neighboring constituents (see their Figure 4).

A measure of the perturbation of μ_2 caused by $2MS_2$ can be determined by subtracting the direct GOT5.5 solution for μ_2 from the linear tide as inferred from $2N_2$ and N_2. The result is shown in Figure 1. Large (off color-scale) amplitudes in shallow seas are expected for $2MS_2$, but the figure also shows amplitudes exceeding 1 cm in much of the open ocean. The tidal signal shown in Figure 1 would be neglected if μ_2 were inferred, thus emphasizing the importance of direct estimation for this constituent. These results also indicate that further improvements to GOT5 tide prediction could be obtained by considering other nonlinear perturbations. An important one, neglected for now, is likely to be perturbations of L_2 by the compound $2MN_2$.

As noted, whether minor constituents are best determined directly or by inference is dependent on several criteria. Some of these criteria—e.g., the lengths of time series and the satellite sampling characteristics—depend on whether one is referring to the T/P-Jason domain (latitudes ±66°) or to polar seas. These must generally be handled in different ways: what can be done with T/P-Jason data cannot always be done with other satellite data. In the polar regions, only the CryoSat-2 satellite has decent tidal sampling as all other polar-flying satellites are sun-synchronous. The region is also limited by sparse data owing to persistent ice. Thus, in polar regions a greater reliance on inference of smaller constituents was found to be necessary, and some minor constituents simply cannot be mapped with any reliablity. This is surely one area where a long SWOT time series will eventually be invaluable.

3 Satellite Altimeter Data

The most important altimeter datasets used for the development of GOT5 are the long series of 10-day measurements[2] obtained from missions Topex/Poseidon, Jason-1, Jason-2, Jason-3, and Sentinel-6A Michael Freilich. In addition, CryoSat-2 measurements have been heavily used over polar regions. The series of altimeters launched by the European Space Agency—ERS-1, ERS-2, Envisat, Sentinel-3A, Sentinel-3B, as well as the SARAL mission, launched by ISRO and CNES—are less useful for tide work because of their sun-synchronous orbits, but some of those data have been used here to help map lunar tides in some regions.

Access to the non-NASA altimeter data has been greatly facilitated by the Radar Altimeter Database System (RADS). RADS was first developed at the Delft University of Technology (E. Schrama et al., 2000; Naeije et al., 2000) and is now mostly maintained jointly by NOAA and EUMETSAT (Scharroo et al., 2013; Scharroo, 2024).

3.1 Four Major Domains

GOT5 has been developed over four partially overlapping domains. In each domain different processing strategies and different data were used to best exploit the advantages or avoid the disadvantages of each altimeter. The overlap regions were used to blend the independent solutions in each domain. Some of these blends were more successful than others; close examination (especially if computing gradients) can sometimes reveal these transitions.

Not all altimeter data were used in all locations. The deep ocean covered by the $\pm 66^\circ$ latitude range of Jason altimetry was restricted to those data alone. In fact, over this domain I also left out T/P altimetry, for reasons discussed below. I certainly see no reason to use the sun-synchronous altimeters in this domain; over time I have noticed many cases in which sun-synchronous data corrupt more accurate estimates from T/P-Jason. However, a variety of altimeter sources, including sun-synchronous ones, were used in higher latitudes as well as in shallow water everywhere.

Table 2 shows the four domains and it summarizes which data were used in each domain.

Figure 2 summarizes where data from each satellite (except CryoSat-2) was used.

Analysis bin sizes must be relatively small in shallow water to capture the high-wavenumber tidal features encountered there. It thus becomes critical to employ as much altimeter data as possible in these locations. This added data density is apparent in Figure 2, and a zoom view around Alaska (Figure 3) shows the data coverage in more detail.

A more informative view of the SARAL coverage in the Arctic and Antarctic is shown in Figure 4, where one readily sees the impact of persistent ice cover that significantly reduces the number of valid ocean returns.

As part of this initial discussion of sources of altimetry, it is useful to delve in greater detail into several topics related to Topex altimetry and CryoSat-2 altimetry. The former deals with a long-standing issue of Topex versus Jason altimetry. The latter is needed because of the different ways CryoSat-2 data have been employed here.

[2]Actual repeat period has been 9.9156 days.

Table 2: Solution domains used to construct GOT5.

Domain	Latitude extent	Satellites	Time span	# days
Main	±66°	Jason, S-6	2002–2023	7924
		Interleaved T/P-J	2002–2023	2961
		GFO	2000–2008	2459
		Envisat, SARAL	2002–2016	4280
		Sentinel-3A	2016–2023	2847
		Sentinel-3B	2018–2023	1860
Arctic	60°–90°N	CryoSat-2	2010–2021	3933
		GFO	2000–2008	2474
		Envisat	2002–2012	3502
		SARAL	2013–2022	3445
Antarctic	79°–60°S	CryoSat-2	2010–2021	3933
		GFO	2000–2008	2401
		Envisat	2002–2012	3502
		SARAL	2013–2022	3447
Ice shelves	86°–65°S	CryoSat-2	2010–2022	4285

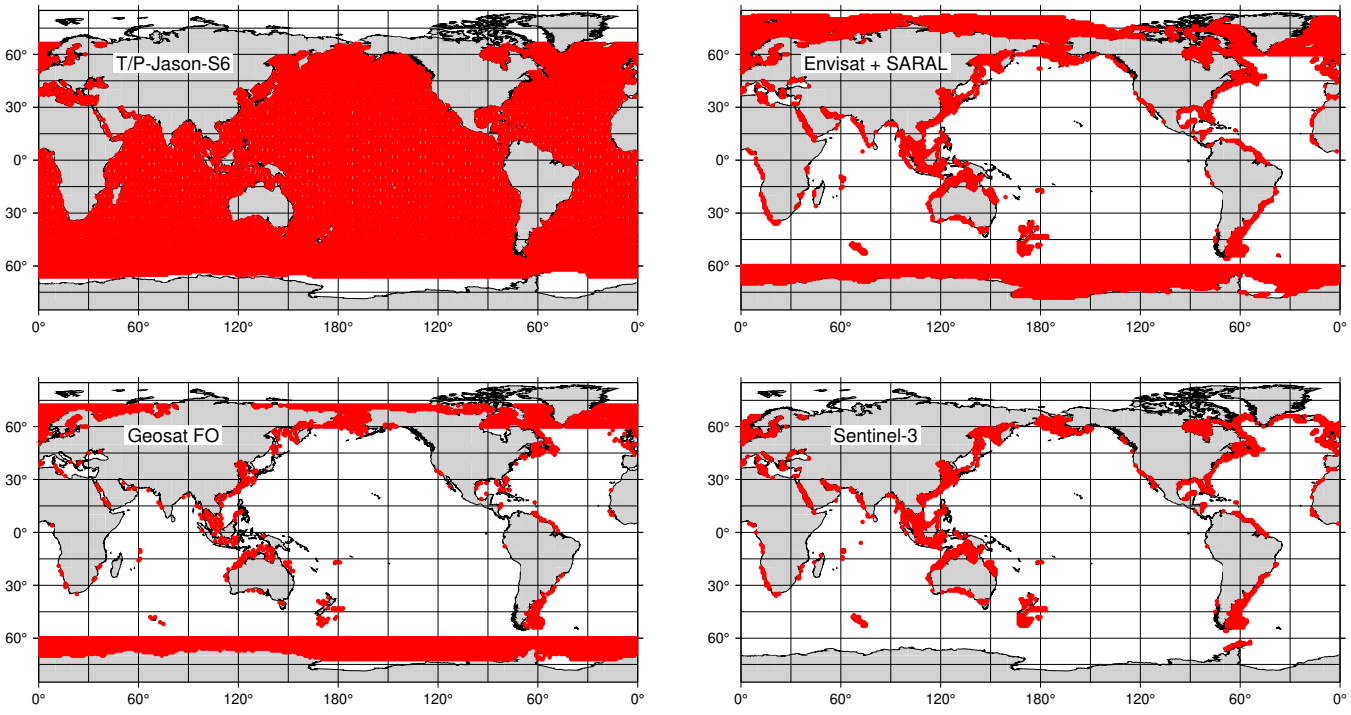

Figure 2: Ocean locations where altimeter data from each satellite series was used in development of GOT5. ERS-2 data were also used wherever Envisat data were.

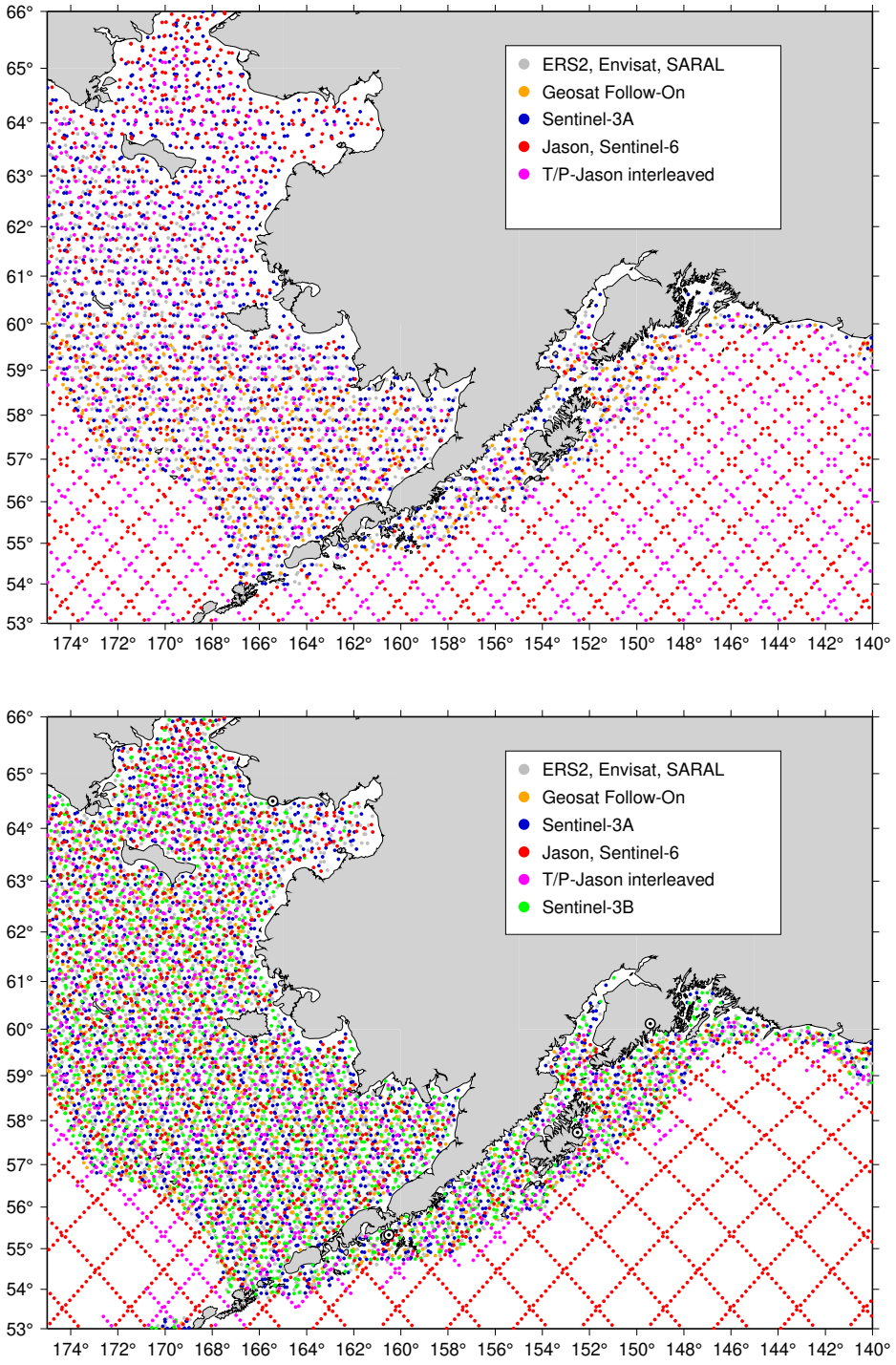

Figure 3: Data coverage from multiple exact-repeat mission satellites around Alaska for (top) GOT5.1 and (bottom) GOT5.5. Each spot was repeatedly observed during each repeat cycle, as along-track interpolation was used to maintain consistent locations for the tidal inversions. Note that the T/P-Jason interleaved data were not used in the deep ocean in GOT5.5; this may or may not have been a good idea—see discussion in text.

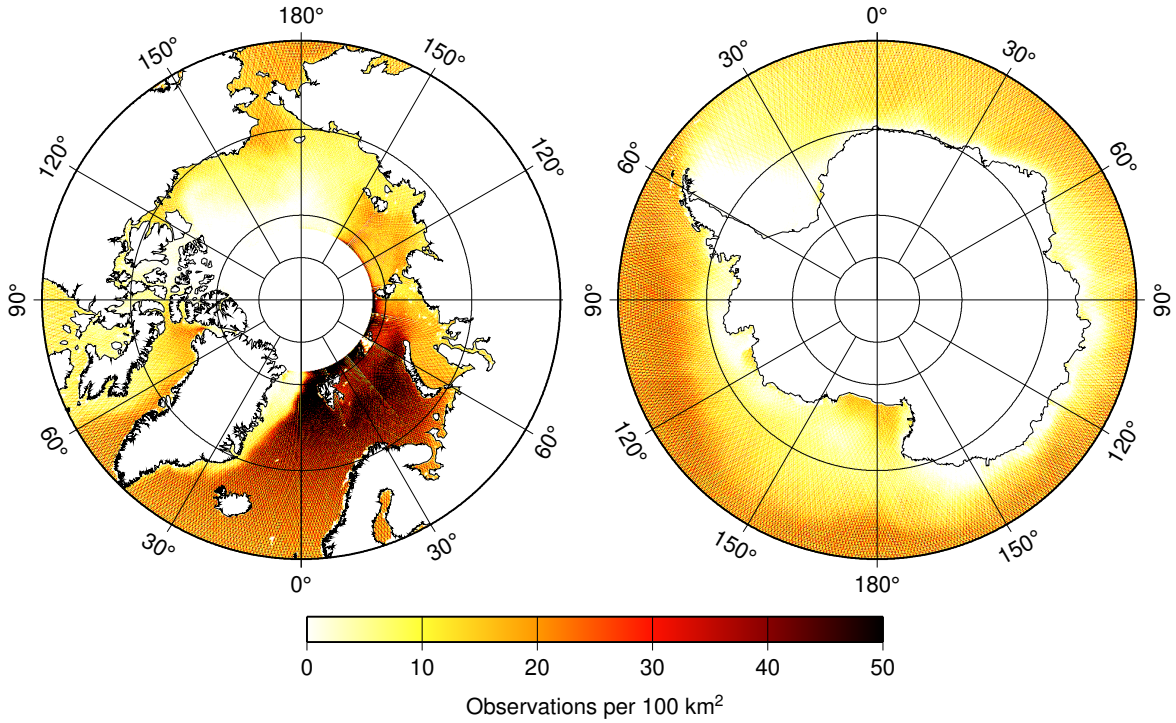

Figure 4: Data coverage of valid ocean measurements for the SARAL satellite over the Arctic and Antarctic Oceans, 2013–2022. SARAL was in a drifting orbit after July 2016.

3.2 Topex/Poseidon β' bias

This section discusses a long-standing problem that results in a small inconsistency in T/P and Jason solutions for the S_2 constituent. Because the problem is thought to rest with T/P, and because we now have two decades of altimetry from Jason and Sentinel-6, we can afford to leave T/P data out of the tidal solutions for the main GOT5 domain. However, newly retracked T/P data, described by Desjonqueres et al. (2023) and released during the course of the present work, appears to reduce the degree of Topex-Jason inconsistency and thus our approach may warrant revision in the future.

As is well known (e.g., Zawadzki et al., 2018), solar tides from altimetry potentially suffer from small systematic errors not affecting lunar tides. These errors are related to solar (thermal) forcing of both spacecraft and the atmosphere (including even the dry-troposphere correction). The particular problem at issue here was first seen during the Jason-1 "cal/val campaign," during which T/P and Jason-1 flew in tandem formation, with Jason-1 leading by 70 s. The measured sea-surface heights were found to depend on β', the angle between the orbit plane and the Earth-Sun vector, and thus also on local solar time. Figure 5a shows an example using measurements collected during the first 21 repeat cycles of Jason-1. A semidiurnal bias is clearly evident, with peak-to-peak differences of 16 mm, and this bias leads directly to different S_2 solutions from the two satellites.

This S_2 difference was shown explicitly (Ray, 2013) in altimeter solutions GOT4.9 and GOT4.10, with the former based on only T/P data (over the deep ocean) and the latter based on only Jason-1 and Jason-2 data; the two S_2 solutions differed, and their differences with "ground truth" bottom-pressure data were markedly larger for GOT4.9. This therefore pointed to the error being primarily with T/P.

The problem has been investigated periodically over the years, and in some detail during a

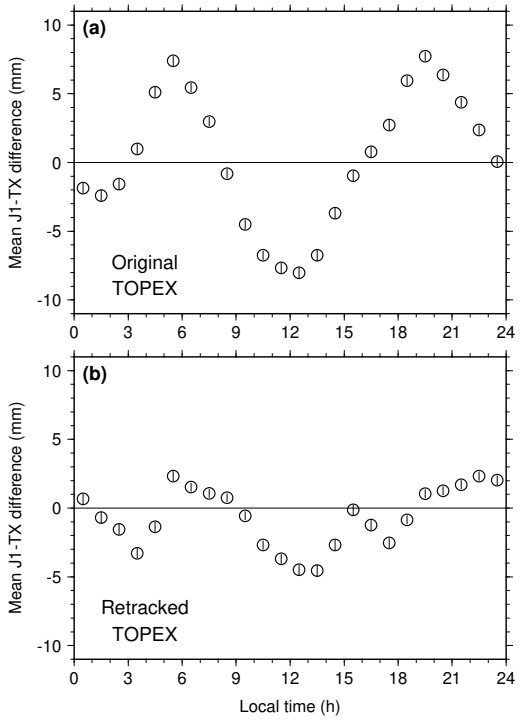

Figure 5: Mean differences in sea-surface heights between T/P and Jason-1, collected during their tandem-flying campaign (the first 21 cycles of Jason-1, January–August 2002) and binned according to local solar time. (a) Original Topex data, with applied C_g correction; (b) newly released retracked Topex data, without C_g. A half-daily local time dependence indicates inconsistency between the two satellites for S_2 tide estimation. Retracked data yield a more consistent but probably not identical S_2 from the two satellites.

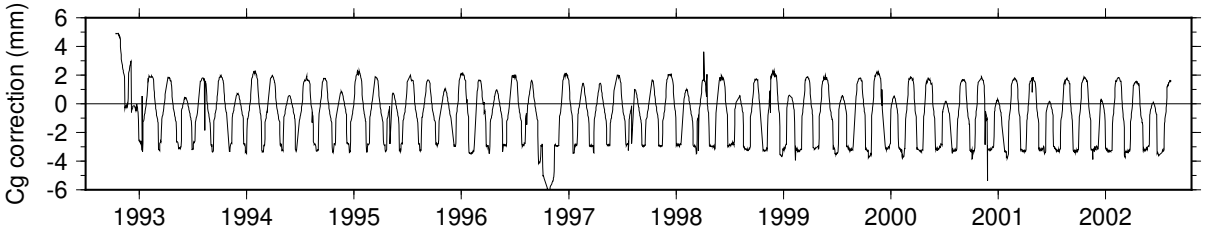

Figure 6: Project-supplied model for the radial motion of the T/P center-of-mass.

special 2010 meeting in Lisbon (e.g., Callahan, 2010; Ablain et al., 2010; Leuliette et al., 2010). The error is thought to have arisen from thermal effects on the spacecraft, which changed according to solar illumination, which in turn changed as the spacecraft was reoriented as its orbit plane precessed (note the T/P precession rate was one cycle in 118 d, or twice the S_2 alias period).

There exists a project-supplied adjustment for T/P center-of-gravity (Cg) motion, dependent in part on thermal flexing of the T/P solar panel, but this correction has always been controversial and deemed inadequate. It is shown here in Figure 6. The main oscillation seen is a 59-day period, reflecting the changes in β'. The magnitude of this correction, whether accurate or not, cannot explain the magnitudes seen in Figure 5a.

Independent modeling of Cg was done many years ago by Kubitschek (1997) and Kubitschek & Born (2001), which was unfortunately never implemented. They developed a model for how the solar array deformed under periodic solar input and showed that Cg varied by up to 2.5 cm peak-to-peak from this flexing, depending on β'. This motion occurred even within one orbital revolution. It is not accounted for in the T/P precise orbit determinations (Frank Lemoine, pers. comm., 2024).

Nonetheless, I can report that the new retracked T/P data evidently reduce the inconsistency

between T/P and Jason-1; see Figure 5b. The improvement is likely due to (at least) two factors: (1) The retracking algorithms better account for spacecraft thermal problems. For example, the altimeter antenna pointing depended slightly on temperature and the solar angle, and the retracking better estimates any mispointing. Some other subtle effects involving thermal perturbation of waveform gates may also have improved (Jean-Damien Desjonqueres, pers. commun., 29 Feb 2024). (2) Turning off the project-supplied Cg correction may be of benefit. In RADS, the Cg correction was applied to the original T/P data by default, but in the updated RADS configuration for the retracked data, it is no longer applied. Figure 5 is based on RADS data, so part of the differences between the two panels arises from this change in the handling of Cg. This nonetheless emphasizes that the inability to accurately model the Cg motion on T/P as it arises from flexing of the solar panel remains an outstanding issue.

The decision to leave out T/P data from the main GOT5 solution was based on Figure 5a. (But the DAC also played a role; see below.) The matter warrants revisiting in the future. Note that T/P data were still used from the interleaved T/P-Jason tracks since those time series are short and also used mostly in shallower water.

3.3 CryoSat-2 Data in Polar Seas

Notwithstanding the "Cryo" in its name, the CryoSat-2 altimeter mission has become an essential element of satellite oceanography, particularly in polar seas that are poorly sampled by other altimeters or are sampled in sun-synchronous mode. For discussions of these data, see Naeije & Bouffard (2021) and references therein. For a useful earlier tide study, see Zaron (2018).

The polar regions (above 66°) in GOT5 rely heavily on CryoSat-2 altimetry, although sun-synchronous altimetry has also been added in places (not always to obvious benefit). CryoSat data were obtained from two sources: (1) RADS, which was used mostly in GOT5.1 and less so later, and (2) a retracked CryoSat dataset, described and distributed by Andersen, Rose, & Hart-Davis (2023) and used in GOT5.5. The retracked data represent an important advance in the use of CryoSat-2 altimetry for tide studies, in both its accuracy and its ease of use. Some discussion of the data available in RADS is still called for here, not only because of its continued use, but also because it extends the time series past the end of the Andersen et al. timespan.

CryoSat-2 in RADS The following description of CryoSat-2 data (C-2) in RADS applies to the RADS database as it existed in August 2022. The database combines the three different operating modes of C-2. The mode mask has changed from time to time, but a typical example is shown in Figure 7. For all valid data existing above 60°N, the Low Resolution Mode accounts for 40% of all data; the SAR mode accounts for 54%; the SARIN mode accounts for the small remainder. The waters of the Canadian Archipelago, where the tides are large and have historically been very poorly mapped, are mostly covered by the SARIN mode.

The SAR data in RADS are in the form of Pseudo-Low Resolution Mode (PLRM), following an algorithm described by Scharroo (2014). This of course degrades the spatial resolution of SAR data, sacrificing some benefits (e.g. Boy et al., 2017), but it thereby creates a mostly consistent type of ocean dataset for the whole CryoSat-2 mission, conveniently handled as any other mission in RADS. Nonetheless, the three operating modes in RADS still differ in some respects and they must be treated differently, especially for data editing.

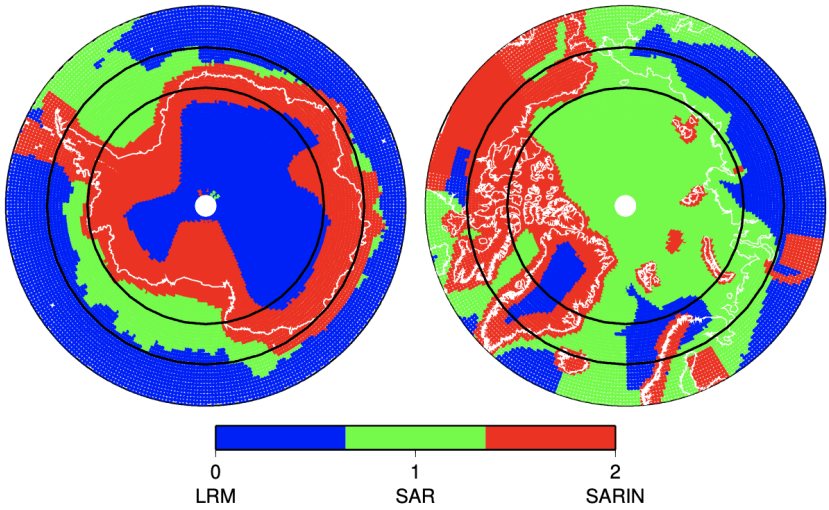

Figure 7: CryoSat-2 altimeter operating modes during cycle 128 (early 2020). The geographical pattern has been modified from time to time throughout the mission. LRM: Low-Resolution Mode, which is comparable to the operating mode of historical nadir altimeters. SAR: Synthetic Aperture Radar, in which coherent echoes are combined into higher resolution by a delay-Doppler approach. SARIN: in which two radar echo chains are used in cross-track inferometric mode. The SARIN mode has been used in many coastal zones and also throughout much of the Canadian Arctic. Heavy black lines mark latitudes 66° and 72°, which are the maximum extents of T/P-Jason and Geosat, respectively.

One useful editing parameter is the waveform "peakiness," which is also used in the current RADS configuration files (default limits 0.0–1.6). Figure 8 shows how the CryoSat-2 peakiness changes for ocean versus ice returns, and as a function of operating mode. The LRM and SAR modes generally have a peakiness less than 1 when reflecting off the open ocean, with ice returns much higher. Figure 9, however, suggests that SARIN mode is likely giving ocean returns when the peakiness parameter is much higher, around 3 or so. Thus, relaxing the default RADS editing for peakiness can result in many more (presumably) ocean data for SARIN, which is helpful for the data-sparse Canadian Arctic.

Figure 10 shows the RADS coverage of C-2 in the polar oceans. Like the SARAL coverage, the C-2 coverage suffers in many regions from persistent ice. Some of the odd patterns in Figure 10, such as seen in the North Atlantic, are related to the different C-2 tracking modes. In many ocean locations, the lack of RADS data seen in Figure 10 prevents reliable estimation of tides.

Retracked CryoSat-2 from DTU GOT5.5 relies heavily on retracked C-2 data as described in detail by Andersen, Rose, & Hart-Davis (2023). The released data have been partially processed to form mean elevations on a semi-regular grid, so the usual track orientation of altimeter data has been lost. The resulting data coverage, displayed in Figure 11 is far more uniform that the coverage available in the PLRM RADS database. In particular, the coverage is now sufficient to support tidal inversions in places not previously attempted. The northern Weddell Sea and (some of) the Canadian Arctic passageways are important examples, as both places are found to have significant offsets from the FES2014 prior.

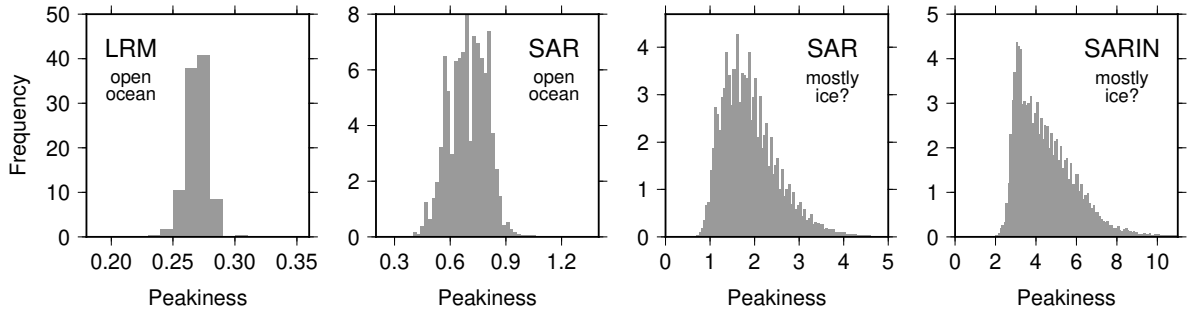

Figure 8: Histograms of the CryoSat-2 'peakiness' parameter by operating mode and environment. The third panel uses data from the region 80°–90°N, 160°–200°E, and is therefore mostly showing returns off ice. The fourth panel is mostly data from the Canadian Arctic, and thus also represents mostly ice returns. The latter data, partitioned by month, is shown in Figure 9.

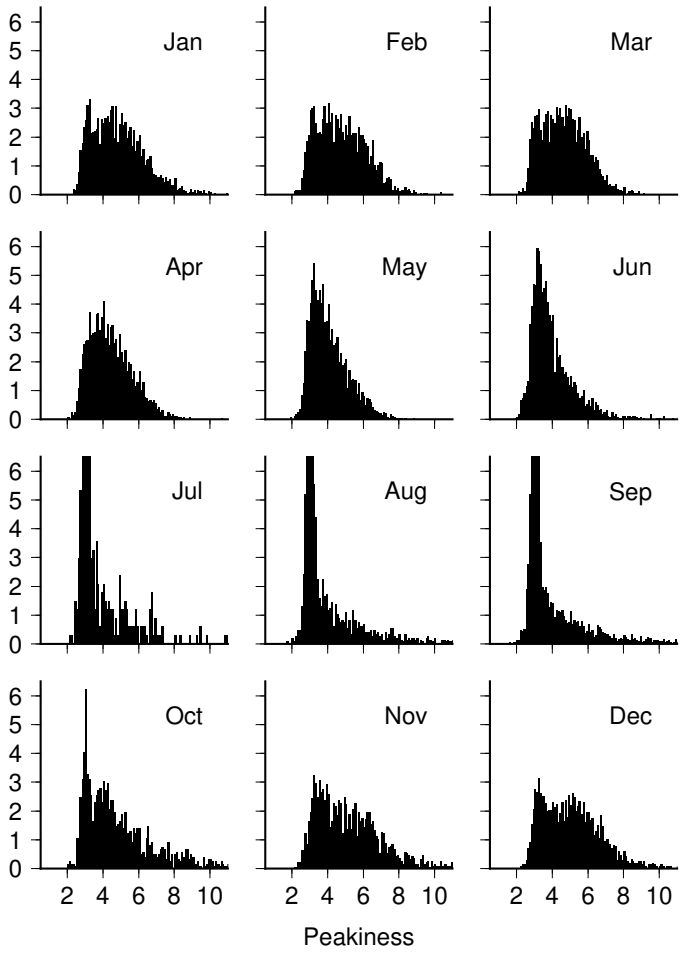

Figure 9: Histograms of the CryoSat-2 'peakiness' parameter for the SARIN operating mode, by month, for data from the Canadian Arctic. Vertical axis is percent of data. Presumably the large peaks around peakiness = 3 during summer months represent ocean reflections, since a good part of the Canadian Arctic has reduced sea ice in those months.

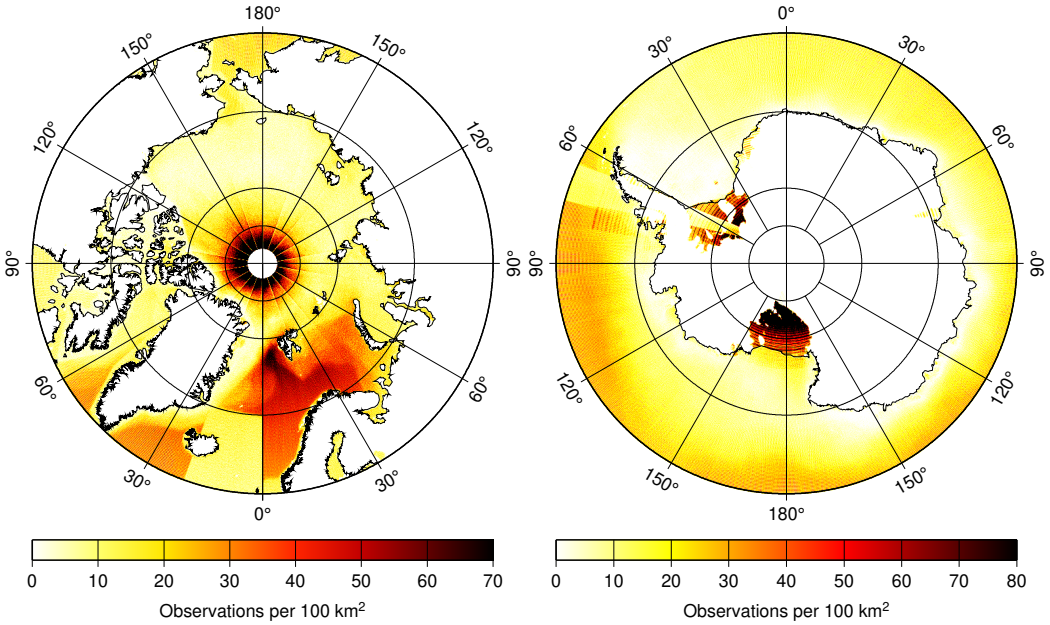

Figure 10: Data coverage in RADS of valid elevation measurements for the CryoSat-2 satellite over the Arctic and Antarctic Oceans.

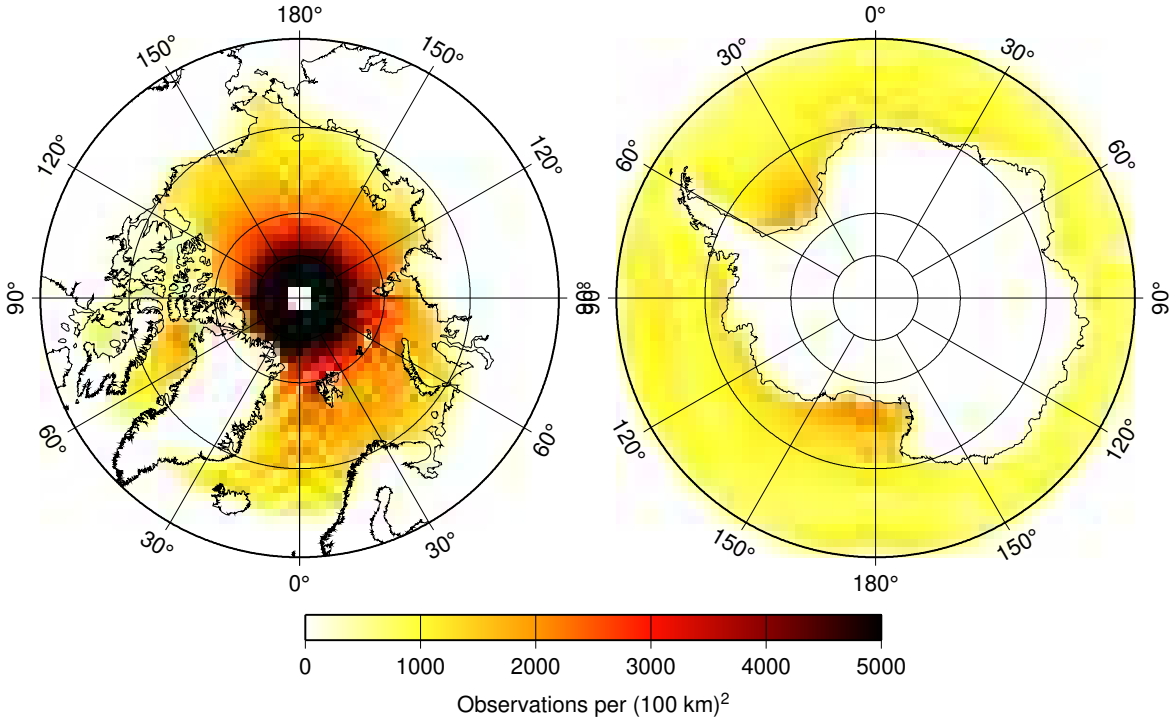

Figure 11: Data coverage of valid retracked ocean measurements for the CryoSat-2 satellite over the Arctic and Antarctic Oceans. Data distributed by Andersen, Rose, & Hart-Davis (2023).

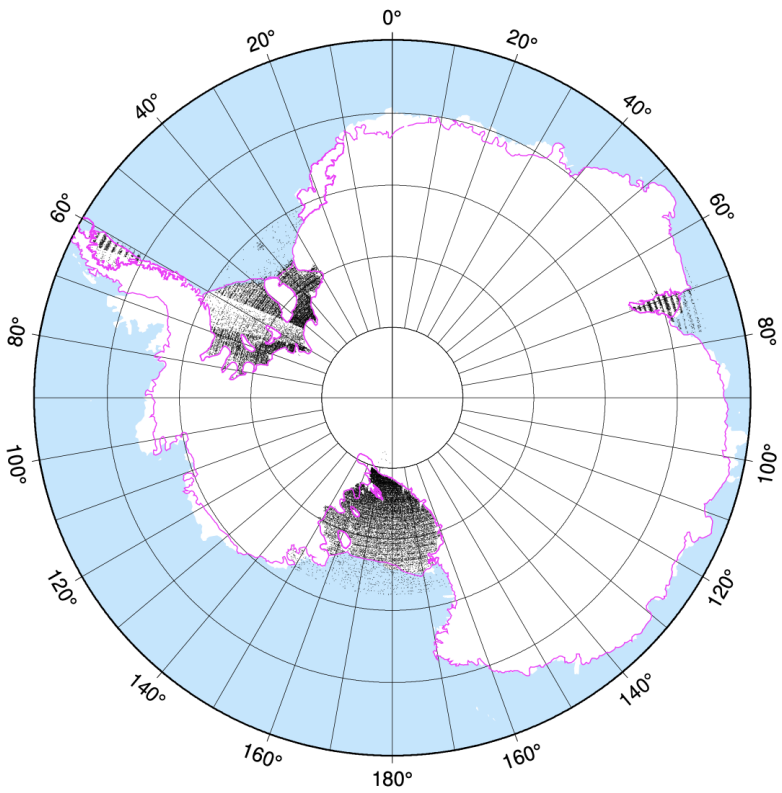

Figure 12: Locations of CryoSat-2 cross-overs (small dots) used for tidal solutions over major Antarctic ice shelves. These data were all obtained with SARIN tracking mode. (To reduce plot size, not every cross-over has been plotted.)

3.4 CryoSat-2 Data over Ice Shelves

GOT5 solutions have also benefited significantly by using CryoSat-2 data over Antarctic ice shelves. These have been in the form of cross-over differences, somewhat similar to that used earlier for ICESat data (Ray, 2008). Cross-over differences have been limited to 2 days or less in time difference in an attempt to minimize changes in the ice elevations between any two observations. Locations of cross-overs are shown in Figure 12.

As the figure indicates, some minor ice shelves have been neglected, and the coverage over some is less than ideal. Further effort is therefore warranted to improve the data density for these important tide regions. Since a relatively small amount of ICESat data have also proven useful in past tide studies (Ray, 2008; Padman et al., 2008), some effort should also be devoted to incorporating the much larger quantities of ICESat-2 data into tide solutions. The different aliasing properties of two satellites (neither of them sun-synchronous) would also be useful in tide inversions.

4 Prior Tide Models

This section discusses both the prior ocean tide model, as used in the remove-restore inversion methodology, as well as the model for solid tides. Any errors in the latter are absorbed into the final ocean-tide solution.

4.1 Body Tides

Most of the altimeter community has been computing height corrections for the body tide by the same algorithm developed for the Geosat mission in the mid-1980s. (An exception is the ICESat-2 project, which follows the IERS 2010 Conventions.) It has been realized for some time that the 1980-era algorithm is not sufficiently accurate, but it has not been updated by project GDR teams, in part because the ocean tide models have been developed with the same algorithm and the desire was to maintain consistency between body tide and ocean tide. I have taken the same route here, but the community eventually needs to move forward.

The body tide algorithm currently used by the altimeter community (again with the I-2 exception) is based on the harmonic expansion of the astronomical potential by Cartwright & Edden (1973), with coefficients extrapolated to year 2000. The Cartwright expansion is still more than adequate for processing satellite altimeter data (if no longer adequate for, say, superconducting gravity measurements). The problem arises with the adopted Love numbers. These have been set to $h_2 = 0.609$ and $h_3 = 0.291$ for all frequencies with the exception of K_1 and its two neighboring nodal lines, which use $h_2 = 0.520$—a crude approximation that only partially accounts for the diurnal resonance effect of the fluid core. These Love numbers are no longer sufficiently accurate. The value of 0.609 apparently comes from Wahr (1981), whose Love number tables give that value for use in the semidiurnal band. Yet Wahr gave 0.606 for the long-period band and 0.603 for O_1 and Q_1 in the diurnal band. Near the diurnal resonance he gave 0.581, 0.520, 0.937, 0.611 for P_1, K_1, ψ_1, J_1, respectively. The Love number error in ψ_1 (which is the closest constituent to the core resonance) exceeds 50%, but because ψ_1 is such a small constituent, the error in tidal prediction is less than 0.5 mm. The most important error for prediction is probably P_1, where the 5% Love number error scales to about 1.6 mm elevation error, far too large to be acceptable. This P_1 error is thus embedded in the current GOT5 solutions.

Use of the IERS Conventions for the body tide is a reasonable alternative. (For P_1 the Conventions give $h_2 = 5817$, ignoring small out-of-phase and degree-4 components, a value close to the Wahr value of 0.581.) But these too could now be updated with more recent models of mantle rheology. Moreover, the IERS's released subroutine for evaluating the body tide is objectionable because it includes a small $(l, m) = (2, 1)$ component for the core-resonance effect in the *load* tide, based on an unknown ocean tide model (possibly Richard Eanes's early T/P solution, CSR3 or CSR4).

At this point, it is clear that the body-tide algorithm used for satellite altimetry needs updating, but its exact form is under debate. The current algorithm generates small errors in the GOT5 ocean tide, notably for P_1, which could impact some geophysical investigations.

4.2 Ocean Tides

The prior model for the ocean tides is here mostly based on FES2014b of Lyard et al. (2021). In a handful of localized near-coastal spots, the model has been patched (e.g., Albemarle Sound—see below). The FES2014 model was developed on a high-resolution finite-element grid, but the released amplitude and phase data are on a finite-difference $(1/16)^\circ$ global grid. Because my empirical analysis of present-day altimetry cannot exploit such high resolution, the grid has been cut back to $(1/8)^\circ$, automatically sacrificing some of the FES2014 accuracy. Thus, a valid question to be addressed in testing (Section 7) is whether this empirical adjustment to FES2014 is making

the tidal atlas better or worse!

The FES2014 atlas does not include all constituents selected for GOT5 (see Section 2), specifically it leaves out σ_1 and OO_1 on the edges of the diurnal band. For these two constituents, a prior has been inferred by linear extrapolation of admittances: σ_1 from Q_1 and O_1, and OO_1 from O_1 and K_1 (accounting for Love number differences in the latter).

Not all the adopted constituents from FES2014 benefited from data assimilation. In particular, J_1 is a purely hydrodynamic solution, and this is reflected in its accuracy (see below). This inconsistent treatment of constituents has an important implication: it would be inadvisable to use a response tidal analysis on the altimeter FES2014 residuals, since the admittance of the residual tides can no longer be a smooth function of frequency.

In a few spots, inadequacies in FES2014 are readily apparent and these spots have been patched. The tide models used for patching are the ADCIRC model EC2015 and ENPAC15 databases (Szpilka et al., 2016, 2018) and the CATS2008 model (L. Padman, pers. comm., 2008; used only in the southernmost Ross Sea). One such patch located along the U.S. east coast will now be described in some detail.

4.2.1 Albemarle-Pamlico Sound

Albemarle and Pamlico Sounds are separated from the Atlantic Ocean by a long chain of barrier islands stretching along much of the coast of North Carolina (Figure 13a). Pamlico Sound is the larger system. It is enclosed by the Outer Banks, which contains Cape Hatteras National Seashore. The barrier islands shut out most of the Atlantic tide, with considerably reduced tidal amplitudes within the sound. This is confirmed by tide gauges in the region.

The FES2014 model appears to have tidal amplitudes too large within the sound, so I have patched in the model values from the ADCIRC EC2015 database Szpilka et al. (2016). (Note the new FES2022 also has large amplitudes in the sound; see Figure 13c.)

The tide gauges listed in the table (Figure 13b) are mostly NOAA gauges, but the Currituck Sound gauge is from the USGS, and one of the Hatteras gauges is from the U.S. Coast Guard. The harmonic constants for half the listed gauges are taken from NOAA tabulations.[3] I have computed the constants for Currituck, Frog Island, Edenhouse Point, and Lake Worth; the last three are only a few months long, but more than adequate to confirm the small tidal amplitudes behind the barrier islands. It is possible, of course, that breaches in the barrier islands change over time, which could lead to changes in the observed tide inside the sound.

The tide gauge at Duck sits on the Atlantic side, with M_2 constants of (47.4 cm, 358°). Duck is normally considered a very good validation site for modeling, but unfortunately the spatial resolution of GOT5 (1/8°) is too coarse to detect the barrier island, so any interpolation of constants done for GOT5 near the Duck location uses data from both sides of the island, resulting in a large error. This includes interpolation done by the `perth5` prediction software (Section 8). The prediction software could be modified to account for the existence of narrow barriers, but this has not been attempted for `perth5`.

A USCG tide gauge at Hatteras, located on the bay side, is probably less useful for validation because it sits close to a break in the barrier island where the Atlantic tide flows into the sound.

[3] `https://tidesandcurrents.noaa.gov/harcon.html?unit=0&timezone=0&id=8653215&name=RODANTHE%2C+PAMLICO+SOUND&state=NC`, accessed Dec. 2024.

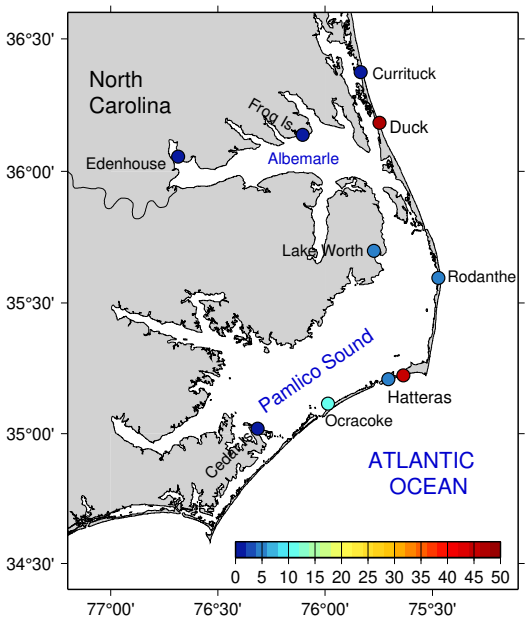

(a) Pamlico-Albemarle Sound

Tide gauge	B/O	Location	H	G
Currituck Sound	Bay	36.37°N, 75.83°W	0.2	198°
Duck	Ocn	36.18°N, 75.75°W	47.4	358°
Frog Is.	Bay	36.14°N, 76.11°W	0.6	182°
Edenhouse Pt.	Bay	36.05°N, 76.68°W	1.8	270°
Lake Worth	Bay	35.70°N, 75.77°W	4.5	88°
Rodanthe	Bay	35.59°N, 75.47°W	5.3	87°
Hatteras	Bay	35.21°N, 75.70°W	4.2	37°
Hatteras Pier	Ocn	35.22°N, 75.64°W	45.3	353°
Ocracoke	Bay	35.12°N, 76.00°W	10.5	6°
Cedar Is.	Bay	35.02°N, 76.32°W	0.6	112°

(b) Amplitudes H (cm), phase lags G at tide gauges

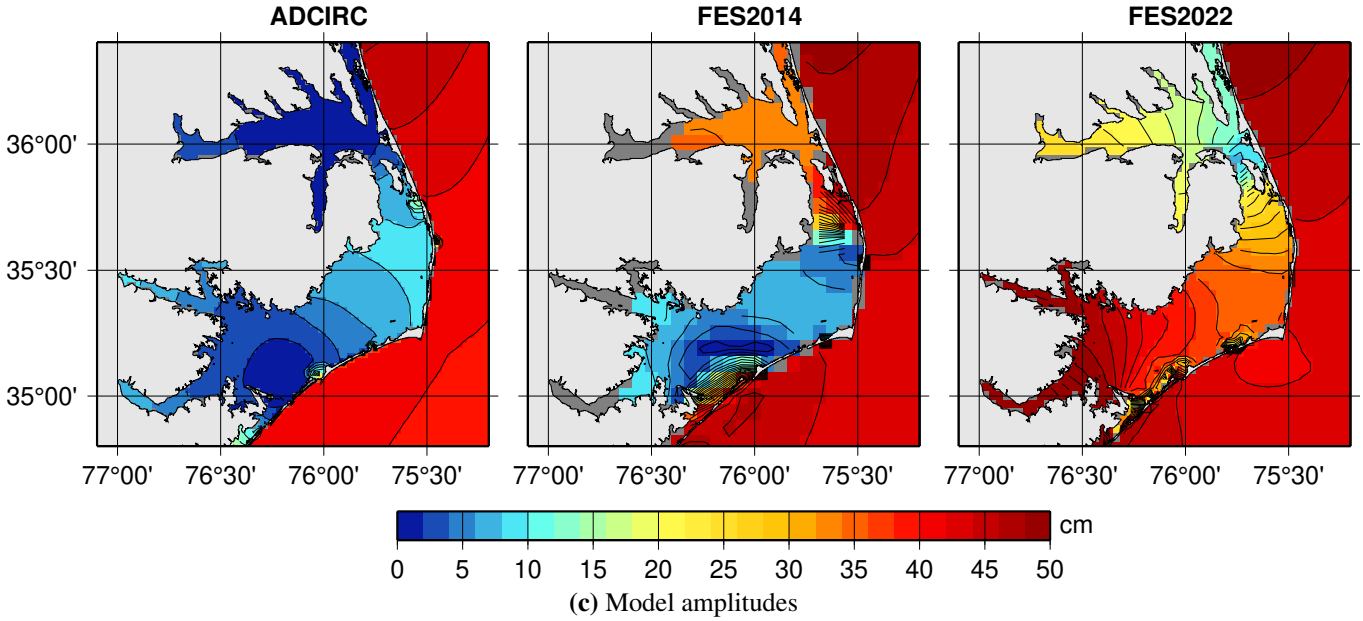

(c) Model amplitudes

Figure 13: M_2 amplitudes in Pamlico-Albemarle Sound

While its small amplitude reflects the tide inside the sound, its phase is closer to the Atlantic tide, with high water occurring nearly two hours earlier than high water at Rodanthe. There was once a tide gauge at Hatteras on the ocean side, called Cape Hatteras Fishing Pier, although not operational since 2003. Its constants are (45.3 cm, 353°), close to the Duck constants, with high water an hour or so earlier than the bay side at Hatteras but with an amplitude ten times larger.

The ADCIRC and FES2014 models both display reduced amplitudes inside Pamlico Sound, with FES2014 in somewhat better agreement with the measured tide at Rodanthe. The models diverge to the south, probably owing to differences in the locations and sizes of the most significant channels connecting the sound and the ocean. The two stations Ocracoke and Cedar Island are not located near the point of greatest model divergence, but both are closer to the ADCIRC amplitudes. In Albemarle Sound the FES2014 amplitudes are much too large, exceeding 30 cm, whereas the tide gauges imply that the true tide is small, and smaller than the Pamlico tide. The ADCIRC model captures this.

4.3 Load Tides

The load tides distributed with GOT5 are not actually "prior" models, but information about them conveniently fits into this section.

First, initial load tides were (re)computed for all adopted prior constituents. These were computed in a center-of-mass reference frame (Desai & Ray, 2014), appropriate for analysis of satellite altimetry with orbits computed in the same frame. The degree-1 loading Love number was taken as $h'_1 = -1.290$. The crustal loading was considered purely elastic (real Love numbers), even though some interesting geodetic measurements are starting to reveal anelastic effects. The calculations were done by high-degree spherical harmonic expansions; in keeping with the (1/8)° grids of GOT5, the degree of expansion was taken to $N = 1440$. Although a Green's function approach is generally more accurate near coastlines, the error from using spherical harmonics is acceptable because the ocean tides themselves are far from perfect near coastlines.

Unlike the body tide, the final GOT5 ocean tides do not depend on these precomputed load tides. The estimated tidal solutions are considered to be adjustments to the prior ocean + load tide, and new load tides are subsequently computed from these summations. The methodology is an iterative one and is laid out in an appendix to Cartwright & Ray (1991). In this work, two iterations were computed to determine the final load tides, and thus the final ocean-tide solutions.

4.4 Internal Tides

The altimeter data over the main domain were also corrected for phase-locked internal tides. The model used for this was HRET14, described by Zaron & Elipot (2024). In most of the ocean, the GOT5 tidal analysis bins were sufficiently large that internal-tide signals (with wavelengths of order 100–200 km) were mostly averaged out and did not affect the GOT5 barotropic solutions. However, a small number of spots were found to have some 100-km-scale noise, which was subsequently suppressed after applying HRET14.

5 A Few Processing Details

Most of the handling of altimeter data followed standard methods, but a few details are unique to this work and merit longer discussion. In particular, issues involving the DAC (Section 5.3 below) are important, especially so for tidal work, and these issues caused some of the complications that resulted in different GOT5 variants (Section 6).

5.1 Mean sea surface for SARAL and CryoSat

Over the main T/P-Jason domain (inside latitudes ±66°), the tidal analyses were based solely on exact repeat mission data, with along-track interpolation done to ensure a fixed set of locations during every repeat cycle. For these solutions, a datum was estimated for every exact-repeat location simultaneously with tidal parameters. For large analysis bins, this could involve many dozens of datum coefficients. The advantage is that the solutions are independent of any model of the mean sea surface (MSS).

In polar latitudes where SARAL and CryoSat-2 data were extensively used, this approach to datum estimation was dropped. Although CryoSat-2 has been nominally in an exact repeat orbit, but with a very long repeat period, it is treated here as if it is not. And after July 2016, SARAL was in a drifting orbit. To handle these data, a accurate model of the MSS is required, which must be consistent among all satellite missions. For tidal analysis of these data, the only estimated datums were simple biases for each satellite mission.

The DTU21 MSS model (Andersen, Rose, Abulaitijiang, et al., 2023) has been used throughout in this work. This surface is given on a global 1-minute grid. The RADS data come with a variety of MSS models, although not necessarily DTU21, so for several missions a separate correction step was required to handle the switch to DTU21.

Andersen et al. warn that Sentinel-3 data "were too problematic" to incorporate into the derived MSS (because those recent data were temporally inconsistent with the older data that formed the bulk of the MSS), and that the MSS would need to be updated to handle Sentinel-3A and 3B. That is not a problem here because Sentinel-3 data were used only in places where a datum for it was estimated at each exact-repeat spot (see Figure 2).

5.2 Mesoscale correction

Most of the altimeter data were corrected for non-tidal ocean variability by removing daily mean sea-surface heights (SSH) as constructed from multi-mission altimetry by Sánchez-Román et al. (2023). These corresponded to DUACS version DT-2021 grids. The correction was applied only for tidal solutions in the Main domain (see Table 2); in much of the polar regions the DUACS heights are undefined.

This correction markedly reduces noise levels in the open ocean, especially in smaller constituents. On the other hand, it is an extremely risky correction to apply. During construction of the DUACS grids, Sánchez-Román et al. (2023) applied an ocean tide model (specifically FES2014b), which obviously was not perfect, as the work here demonstrates Some of the mismodeled tide can potentially leak into the DUACS SSH grids (Zaron & Ray, 2018), thus removing the FES2014 error

that we are attempting to determine.[4]

Some preliminary tidal solutions were made in order to study this problem, specifically for testing possible leakage in the open ocean. (These tests were part of GOT5.2, a variant of GOT5 that was never released.) One constituent (again in the open ocean) that clearly was degraded by the DUACS correction was M_3—a constituent that is not especially accurate in FES2014, thus potentially inducing rather large leakage errors in DUACS data. Thus, when solving for all four degree-3 tides in GOT5.6, the DUACS correction was not applied.

When applied, the correction is almost certainly degrading the GOT5 solutions in shallow water. A strong suggestion for this degradation can be seen by solving for an aliased M_2 signal in a time series of the daily DUACS grids and comparing the results for several versions. As the T/P-Jason alias period for M_2 is 62.1 days, the amplitude of a sinusoid of this period were extracted from 20 years of DUACS grids, using versions DT-2014, DT-2018, and DT-2021. Figure 14 shows the extracted amplitudes. The large change from DT-2014 to DT-2018 was caused in part by a change from using tide model GOT4.8 to model FES2014 (although the DUACS gridding algorithms also changed). The are more subtle changes from DT-2018 to DT-2021, both based on FES2014. Not all this 62-d signal is necessarily tidal leakage. Yet only signals that remain coherent (phase-locked) over the course of 20 years can appear in this figure, so one must expect much of the signal is indeed tidal. Thus, the "mesoscale correction" is most likely degrading GOT5 results in shallow-water regions as indicated in Figure 14. It was obviously a judgment call as to whether to apply this correction or not, and the noise reduction in the open ocean argued for applying it. I suspect this problem will remain as we begin including new SWOT data into tidal solutions; the SWOT time series is too short to avoid errors from non-tidal variability, and thus some attempts to suppress this noise will be needed.

5.3 Dynamic Atmosphere Corrections (DAC)

The Dynamic Atmosphere Correction (DAC) was developed by Carrère & Lyard (2003), and it has been maintained and upgraded by them ever since (Carrère et al., 2018). The goal of the DAC has been to remove dynamic ocean variability at periods shorter than the nominal T/P Nyquist period of 20 days (and to supply an inverted-barometer adjustment at periods longer than that). It does this by modeling short-period ocean variability with a high-resolution barotropic model, forced by ECMWF winds and pressures. The correction is used in nearly all altimeter investigations (two notable exceptions were the development of the GOT4 and TPXO tide models).

5.3.1 Tidal signals in DAC

The altimeter tide corrections and DAC correction must be applied in a consistent way that avoids any double-counting of ocean signals. It turns out that this is rather difficult to accomplish owing to the problematic nature of atmospheric tides and to unacceptably large errors in most models of these tides (see recent complementary discussions of this topic in Ray & Schindelegger, 2025). Atmospheric pressure tides are the proximate cause of the so-called radiational components of ocean tides (Cartwright & Ray, 1994; Dobslaw & Thomas, 2005; Arbic, 2005), and radiational components are an inherent part of all major existing global ocean tide models. To avoid double-counting

[4]That such ocean-tide model errors are now impacting subsequent tidal investigations does contain a degree of irony. As my colleague Gerald Dibarboure put it, it is a case of the snake biting its own tail.

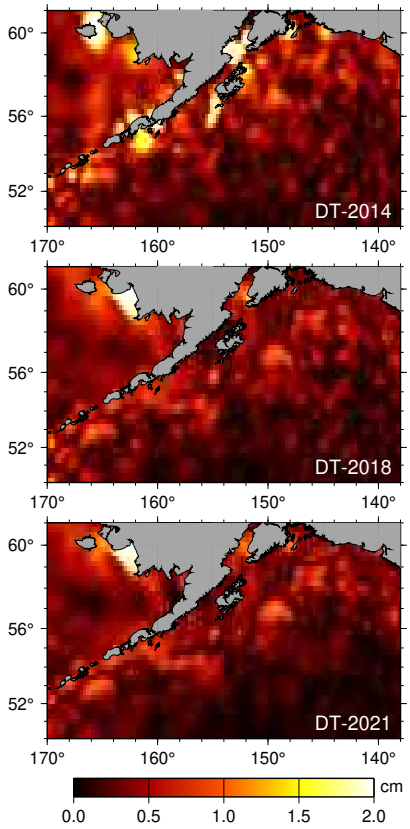

Figure 14: Amplitude of 62.1-day sinusoids (62.1 being the M_2 alias period in Topex-Jason data) as extracted from 20 years of daily DUACS altimeter grids, for three versions (top to bottom: DT-2014, DT-2018, DT-2021). Much of this signal presumably arises from leakage of ocean-tide model errors into the DUACS mapped sea surface heights. DT-2014 used tide model GOT4.8; the others used FES2014. Changes in gridding algorithms in the different versions also affected how tide-model errors potentially leak into the mapped heights.

radiational tides, the DAC correction has been developed to avoid any forcing by atmospheric tides (Carrère et al., 2016), but this avoidance has been only partially successful. The major reason is modeling errors in the atmospheric tides that exist in the ECMWF operational pressures have made their removal unduly complicated, especially if that removal is attempted by developing and applying a climatological model (as advocated, for example, by Ponte & Ray (2002)). Moreover, the current DAC modeling removes only solar air tides; lunar tides have been neglected, probably because they were thought too small to be concerned with. That is no longer the case (Ray & Schindelegger, 2025).

To see the extent that radiational tides—even for the lunar M_2—exist in the DAC, I have estimated tides from the global DAC sea-surface heights. (The DAC data are provided every 6 hours; the S_2 tide therefore cannot be fully determined, although its in-phase component can be.) The extracted M_2 tide is shown in Figure 15. This figure is essentially a depiction of the M_2 radiational tide, a signal now unfortunately embedded in the DAC.

A second unfortunate point is that the DAC tide signals have changed over time. This is easily seen for M_2 by estimating tides from the DAC time series in six non-overlapping five-year windows. The estimated M_2 amplitudes are shown in Figure 16a, where increasing DAC amplitudes are readily apparent. Those increasing amplitudes arise directly from similarly increasing M_2 air-tide amplitudes in ECMWF operational pressures (column b). In particular, the M_2 signals in both are seen to nearly vanish in the early T/P years.

Note that recomputing the DAC by switching to ERA5 reanalysis pressures (Hersbach et al., 2020) rather than operational pressures, will not solve this time dependence, as Figure 16c shows ERA5 amplitudes also increasing, but in different fashion from operational amplitudes. In fact,

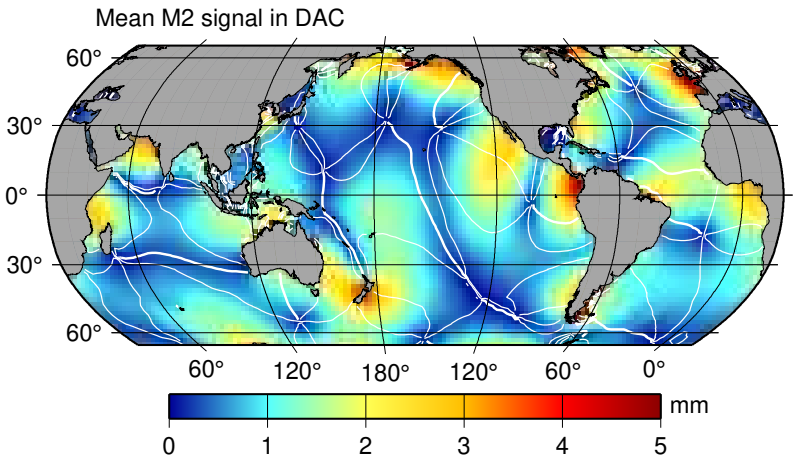

Figure 15: The M_2 amplitudes (in color) and phases (white lines), as extracted from 6-h DAC elevation fields, 1993–2022. This is the ocean's computed response to pressure loading by the ECMWF lunar air tide, based on the numerical model of Carrère & Lyard (2003). This tidal signal is embedded in the current standard DAC altimeter corrections even though some ocean-tide model corrections (e.g., GOT4) also include it.

amplitudes in operational pressures appear to level off after about 2015, whereas ERA5 amplitudes do not (e.g., in column (c) the red spot in the Atlantic is largest in the final 2018–2022 panel).

I will not discuss here similar problems with the (much larger) solar air tides that are in ECMWF data. However, they too have clear errors, similar to some extent to the increasingly energetic lunar tides evident in Figure 16. This is so for both operational and ERA5 reanalysis data. A study by Diaz-Argandoña et al. (2016) shows that spurious, unphysical variations in solar atmospheric tides is an unfortunate feature of the reanalysis products from all major meteorological centers. In fact, according to their work, ECMWF reanalysis tides are perhaps less erratic than those of most other centers (see their Figure 5).

These complications with air tides are unfortunate. Radiational tides are a significant fraction of observed ocean tides—perhaps 20% of S_2, smaller for M_2. Handling radiational tides necessarily involves development and use of models of atmospheric tides. Thus, problematic air tides and their inadequate modeling stand as an outstanding issue for altimeter tide studies.

5.3.2 Some approaches to deal with tidal signals in DAC

The best approach to deal with the problem of tidal signals in the DAC is presumably to modify the methods used to remove air tides in ECMWF pressure data before those pressures are used to force the DAC ocean model. The same problem has been faced by the GFZ (Potsdam) group who supplies the atmosphere/ocean de-aliasing model for GRACE, and they have made some progress on this problem over the years as their de-aliasing corrections have been revised and improved (Shihora et al., 2022). However, their approach, even if eventually adopted for altimetry, will involve further development work and considerable testing—the altimeter time series began well before the GRACE era—in no small part because of the spurious/erratic tide signals that must be handled in reanalysis data. Handling the pre-1997 signals in Figure 16b must differ from how they are handled post-2013. Future attempts to better model tide-surge interactions (e.g., Prandle & Wolf, 1978; Idier et al., 2019), which will become necessary in some places as altimetry is extended ever closer to the coast, will further complicate how these signals are eventually handled.

In the GOT4 models, the DAC was not used precisely because these kinds of air-tide problems were anticipated. Instead a simple inverted barometer (IB) model was applied, based on daily averages of NCEP Reanalysis surface pressures. Forming daily averages removes the bulk of any

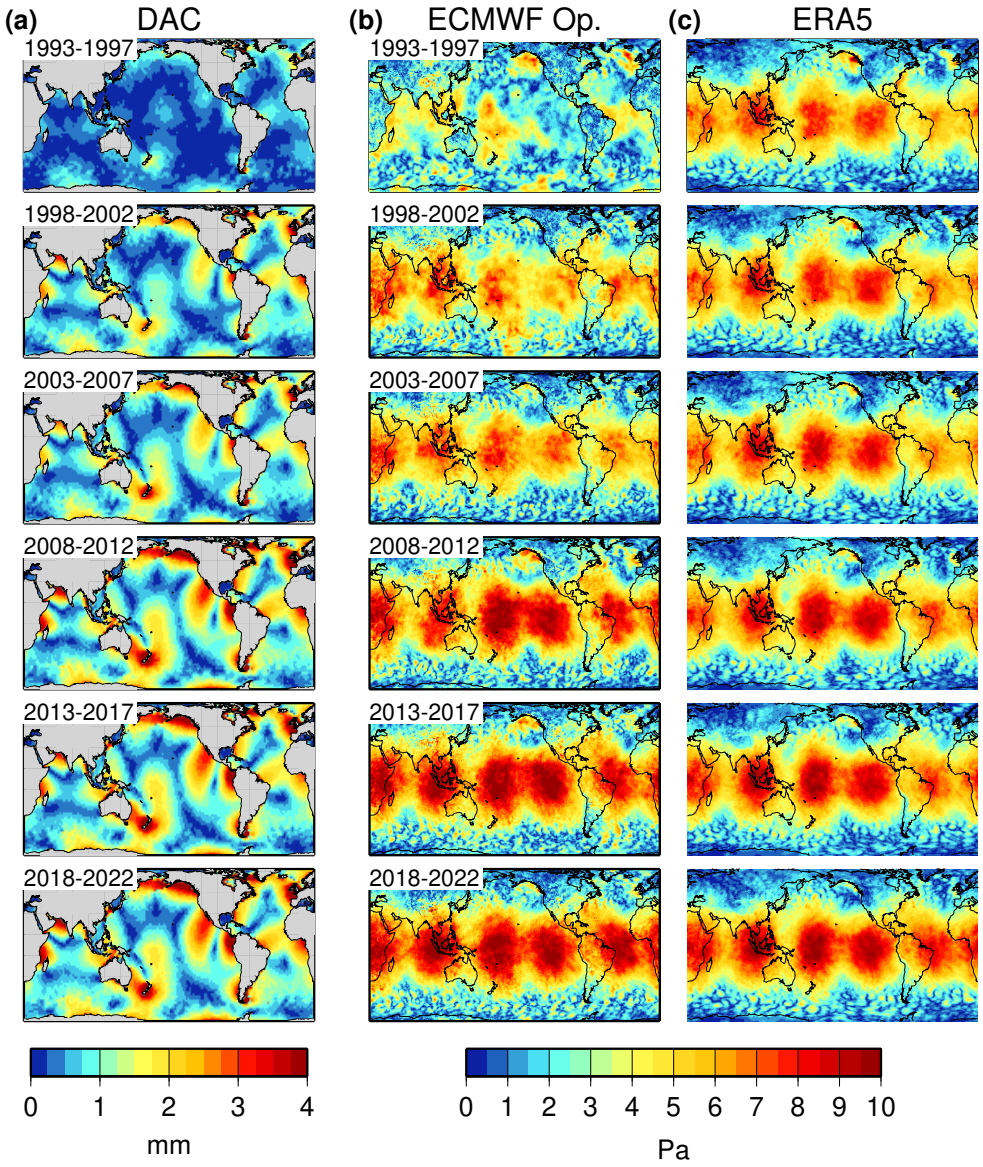

Figure 16: Amplitudes of M_2 tidal signals extracted from 5-year windows of (a) the DAC altimeter correction (Carrère & Lyard, 2003), (b) ECMWF operational surface pressures, and (c) ECMWF ERA5 surface pressures. The DAC SSH fields were originally computed by using the operational pressure (and wind) forcing; the lunar tide signal in these pressures is evidently suppressed before 1998, leading to a spurious trend in the DAC lunar-tide leakage. Yet over the entire 30 years, tidal amplitudes of both operational and ERA5 pressures still appear to increase with time. Both pressure fields are therefore inadequate for studies requiring accurate models of air tides. Data in (b) were kindly computed by Loren Carrère and Perrine Abjean.

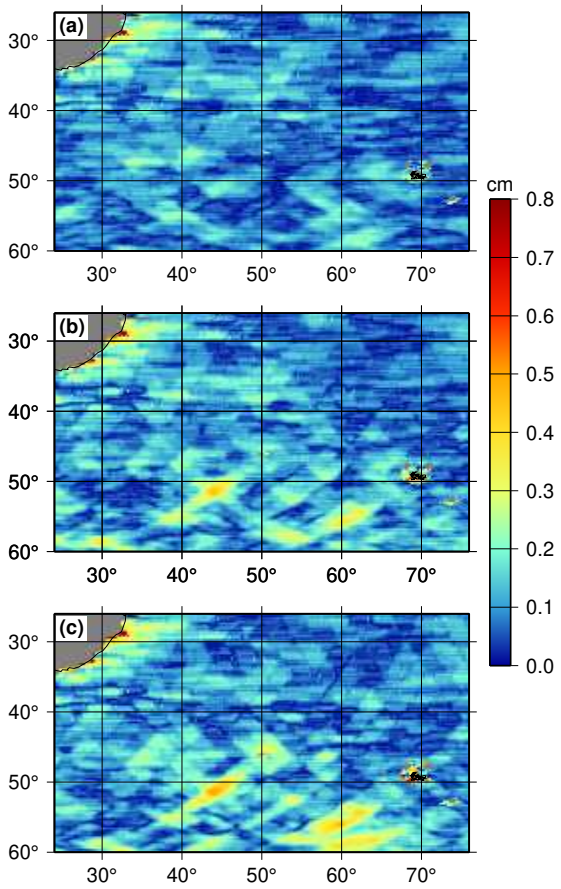

Figure 17: Amplitudes of raw (unsmoothed) tidal estimates from Jason and Sentinel-6A altimetry, relative to the prior FES2014 model, for the M_4 constituent in the western Indian Ocean. In each panel, the altimetry has been corrected for atmospheric loading by using (a) the standard DAC (Carrère & Lyard, 2003), (b) a mean-daily DAC, and (c) a mean daily IB, based on ERA5 pressures. Some trackiness patterns are more evident in panels (b) and (c), which have been better suppressed by using the entire DAC as a correction. However, using the entire DAC means admitting leakage of residual signals from radiational tides.

diurnal or subdiurnal tidal signals,[5] so that GOT4 models properly include the full radiational tide signal. The same approach was used for GOT5.1, except that NCEP Reanalysis pressures were replaced by more accurate ERA5 pressures.

The drawback to the GOT4 and GOT5.1 approach is that a simple IB model is a poor representation of oceanic variability at periods shorter than 20 days. This variability is better captured by the current DAC model (Carrère et al., 2018). The consequence of this is that raw altimeter tide solutions are noisier with an IB correction than with the DAC. This is most apparent in higher latitudes, where pressure-driven variability is most pronounced. An explicit example is shown in Figure 17, which shows tidal solutions for M_4 in the western Indian Ocean; the real tidal signal in this figure is expected to be small, so any evident signal, especially if of short wavelength and displaying a 'trackiness' pattern, is likely noise. Using a mean-daily IB correction, as in GOT5.1, evidently results in considerable residual noise. Forming daily means of the DAC itself results in less noise, but it is still inferior to applying the entire DAC.

Based on this residual noise experiment, GOT5.5 employed the full DAC as the correction for atmospheric loading (as nearly all other altimeter investigations do, too). But it must then face the problem of leakage of radiational tide signals into the DAC.

The leakage problem grew more severe over time—see column (b) of Figure 16, which argues

[5]As is well known (Munk & MacDonald, 1960), forming an average of the M_2 tide over each solar day does leave a small residual, which shows up aliased to the frequency of the MSf constituent (period 14.765 days). The amplitude of this residual aliased signal at MSf amounts to only 4.4% of the original M_2 signal.

Table 3: RMS tide gauge* differences (cm) for tides affected by DAC air-tide leakage.

Version	Used DAC?	M_2	S_2	S_1	K_1
GOT5.1	No	0.305	0.261	0.277	0.239
GOT5.5D	Yes	0.314	0.260	0.300	0.234
GOT5.5	Yes, then adjusted	0.307	0.263	0.293	0.232

* Based on 151 deep-ocean tide gauges; see Section 7.

for treating early altimetry differently from later altimetry. The Topex β' problem already prompted using only Jason and Sentinel-6A data in the main GOT5 domain, and the change in character of the leakage problem reinforces avoidance of T/P just for the sake of maintaining a consistent input altimeter dataset. Once a tidal solution was found, it was then adjusted for the mean tidal signals in the DAC over the post-2002 era (i.e., after Jason-1 was launched). This formed GOT5.5. However, the unadjusted solution would be preferable to use in any altimeter application that also employed the DAC, so the unadjusted tide solution was kept and became GOT5.5D—with the 'D' indicating it is to be used with the DAC, at least for Jason and Sentinel-6 altimetry. In fact, because the DAC tide leakage was less severe for T/P, it might be proposed to use 5.5 for T/P and 5.5D for Jason and Sentinel-6. This is obviously not ideal, but one must accept the fact that the DAC tide leakage has changed over time.

Also less than ideal is that the final tide solution, GOT5.5, may not be as accurate as GOT5.1 in the open ocean, even though it must be benefiting from the reduced noise apparent in Figure 17. This is suggested by some tide gauge tests summarized in Table 3—more complete tests are described in Section 7.

According to Table 3, the adjustment resulting in the final GOT5.5 solution resulted in better comparison with deep-ocean tide gauges than the unadjusted GOT5.5D, except for S_2 which was slightly degraded. However, for three of the four tides, the agreement is poorer than that obtained with GOT5.1 (K_1 is the exception). So even though GOT5.5 must have benefited from lower altimeter noise than GOT5.1, the complications of leaked air tides in the DAC still caused greater errors, except for K_1. The end result of this is that the DAC problem cannot be considered solved by the present approach, and more work is warranted. Of course, the ideal solution would be a revised and recomputed DAC, but that awaits the future.

6 Summary of GOT5 Variants

As a quick synopsis, the following is a quick summary of the major differences between GOT5 variants (as of this writing). Some of these versions were not taken through all processing steps, as they were more experimental than not. All these versions used the same prior tide model(s) and, except as noted, the same data; both priors and data are described in previous sections of this report.

GOT5.1 Atmospheric loading by daily mean IB (ERA5).

Used C-2 from RADS.

Used interleaved T/P-J data everywhere.

GOT5.2 Same as 5.1 but without the DUACS mesoscale correction.

GOT5.5D Atmospheric loading by standard DAC.

Used C-2 mostly from Andersen, Rose, & Hart-Davis (2023).

Used interleaved T/P-J in depths < 2500 m.

Algorithm changes to improve mapping in shallow water.

GOT5.5 Atmospheric loading by standard DAC, then adjusted solutions for tide leakage in DAC.

Otherwise identical to 5.5D.

GOT5.6 Supplements 5.5 with four additional degree-3 tides from Ray (2020).

No mesoscale correction applied for these four extra tides.

For all standard applications requiring information about tides or tidal prediction, it is recommended to use GOT5.6 (including 5.5). When to use GOT5.5D is less clear. Certainly it should be used only for satellite altimeter applications and only when the present-day DAC is applied. Possibly it should be used only after circa year 2000 when the leakage problem in the DAC became more pronounced—see Figure 16a on page 23.

For variance reduction tests on altimeter data, I expect that, except for early T/P data, an application of GOT5.5D + DAC will result in a larger variance reduction than an application of GOT5.5 + DAC. But GOT5.5 gives the more accurate depiction of tides.

7 Tide Gauge Comparisons

This section tests the GOT5.5 tide solution against compilations of harmonic constants determined at tide gauges.

7.1 Global Ocean

For the primary tests the tide gauges, mostly covering the main (latitudes ±66°) domain, are compiled into three separate categories: deep ocean, shelf sea, and coastal. There are 151, 195, and 262 stations, respectively, in each category. The deep and shelf stations are identical to the stations used by Stammer et al. (2014), but the coastal stations are an expanded set. The locations of the tide gauges are shown in Figure 18.

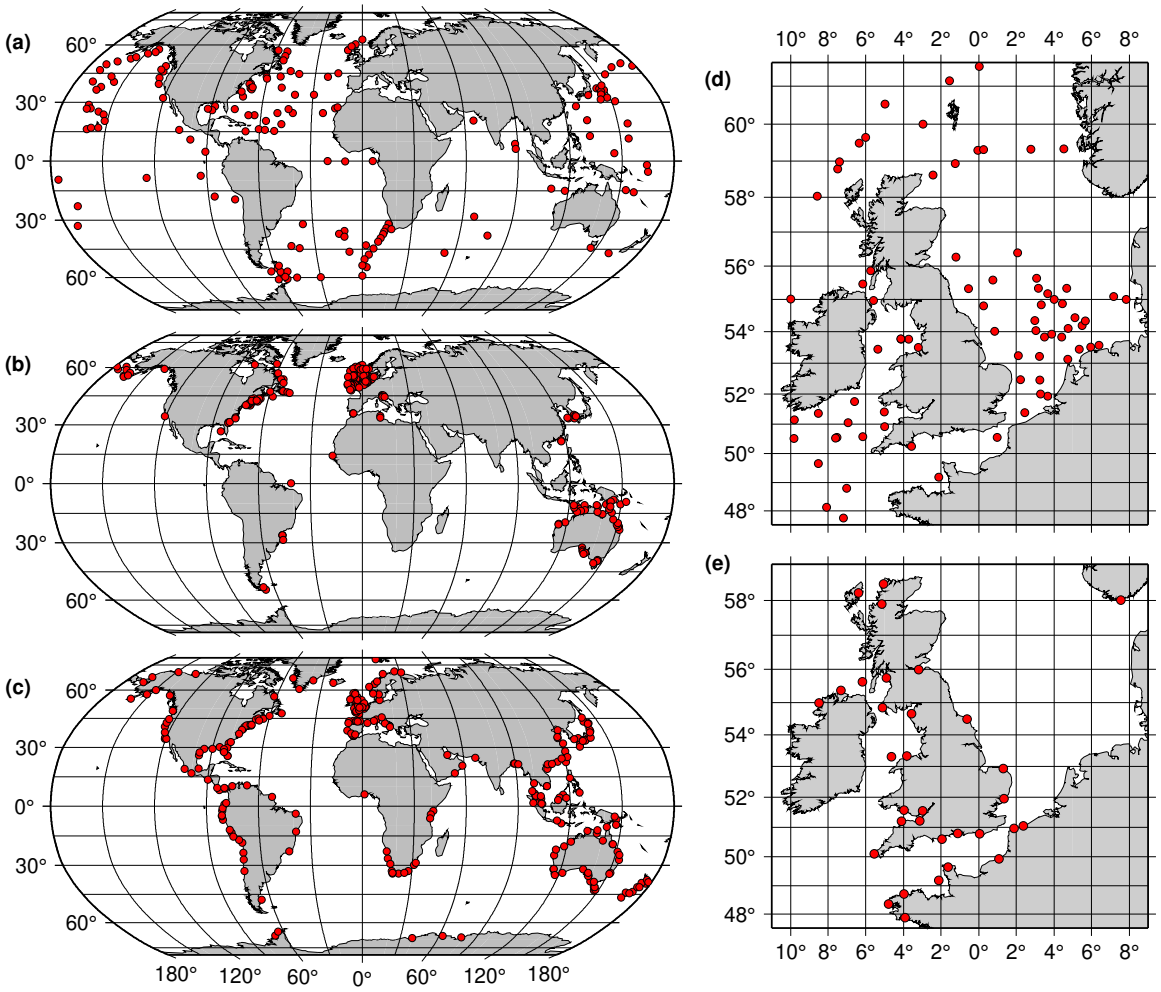

Figure 18: Locations of tide gauges used for model tests: (a) deep, (b) shelf, and (c) coastal stations. Zoom views of the European Shelf show (d) shelf and (e) coastal stations in that region. Some stations in (d) are from fairly short bottom-pressure records obtained in the 1970s and 1980s, some are gauges on oil rigs, a few are small offshore islands. (Close examination of (d,e) reveals one duplicate station: St Helier, Jersey, in the English Channel.)

Table 4: Deep Ocean: RMS differences (cm) with 151 tide gauges.

	Q_1	O_1	P_1	S_1	K_1	J_1	$2N_2$	μ_2	N_2	M_2	S_2	K_2	M_4	MS_4
FES14	0.136	0.181	0.138	0.296	0.227	0.450	0.095	0.096	0.192	0.300	0.266	0.148	0.120	0.128
EOT20	0.297	0.252	0.280	0.498	0.386	0.276	0.190	–	0.346	0.482	0.439	0.328	0.176	–
GOT4.8	0.165	0.296	0.234	0.331	0.423	–	–	–	0.252	0.510	0.369	0.209	0.089	–
GOT5.1	0.131	0.172	0.132	0.277	0.239	0.116	0.092	0.068	0.191	0.305	0.261	0.138	0.054	0.060
GOT5.5	0.133	0.180	0.144	0.293	0.232	0.105	0.086	0.060	0.199	0.307	0.263	0.136	0.041	0.052

Table 5: Shelf Seas: RMS differences (cm) with 195 tide gauges.

	Q_1	O_1	P_1	S_1	K_1	J_1	$2N_2$	μ_2	N_2	M_2	S_2	K_2	M_4	MS_4
FES14	0.79	0.92	0.66	0.88	1.29	0.97	0.54	1.53	1.48	3.47	2.18	0.91	0.65	1.71
EOT20	0.80	0.90	0.71	0.87	1.39	0.80	0.51	–	1.43	3.18	2.11	0.84	0.70	–
GOT4.8	0.82	1.00	0.84	0.90	1.54	–	–	–	1.98	4.88	2.78	1.48	2.23	–
GOT5.1	0.80	0.92	0.70	0.76	1.37	0.80	0.56	1.46	1.45	3.28	2.12	0.86	0.63	1.23
GOT5.5	0.73	0.87	0.64	0.71	1.35	0.78	0.49	1.42	1.39	2.83	1.91	0.77	0.65	1.16

Table 6: Coastal Waters: RMS differences (cm) with 261 tide gauges.

	Q_1	O_1	P_1	S_1	K_1	J_1	$2N_2$	μ_2	N_2	M_2	S_2	K_2	M_4	MS_4
FES14	0.26	0.96	0.50	0.55	1.37	0.63	0.32	1.11	1.71	7.64	3.26	1.06	1.35	1.93
EOT20	0.35	0.94	0.54	0.80	1.29	0.34	0.36	–	1.57	7.04	3.10	0.93	1.26	–
GOT4.8	0.58	1.80	0.92	0.82	2.52	–	–	–	3.61	16.25	9.52	2.48	2.63	–
GOT5.1	0.34	0.94	0.53	0.43	1.37	0.30	0.38	1.11	1.67	7.27	3.17	1.01	1.30	1.57
GOT5.5	0.31	0.92	0.52	0.66	1.42	0.29	0.38	1.06	1.54	6.71	3.02	0.92	1.29	1.44

The 151 deep-ocean stations are all from analyses of bottom pressure recorders (Ray, 2013). The conversion from bottom pressure to equivalent sea-surface height accounted for (climatological) seawater density at each site, based on the temperature and salinity data of the 2013 World Ocean Atlas. The pressures were also adjusted to remove contributions of atmospheric tides for constituents S_1, S_2, T_2, and R_2 (but not M_2); this was done using tidal pressures extracted by my colleague Jean-Paul Boy from 3-hour ECMWF operational pressures for the period 2001–2006.

A large compilation of harmonic constants for coastal stations now exists following work by Piccioni et al. (2019) and M. Hart-Davis et al. (2022). The 262 coastal stations used here are an independently analyzed subset, partly predating those larger collections, based on selected GESLA2 (and later GESLA3) time series data (Woodworth et al., 2017; Haigh et al., 2022). The GESLA3 data now include a number of river and estuary tide gauges which I attempted to avoid for present testing purposes.

The following tables (4–6) give RMS differences between the tide-gauge harmonic constants and various GOT models. I also include RMS differences with model FES2014, since it formed the bulk of the prior for GOT5. If the RMS for GOT5 exceeds that for FES2014, one might conclude I have degraded the latter. This is perhaps true in part, but the story is complicated by the fact that many tide-gauge constants were assimilated into FES2014 (Lyard et al., 2021, their Figure 11), including all 151 of the deep-ocean stations. I also include in the tables the EOT20 model (M. G. Hart-Davis, Piccioni, et al., 2021), because it has consistently performed well in near-coastal tests.

Tide models in the deep ocean, in the latitudes covered by T/P-Jason, have been of high quality

for some time now (Stammer et al., 2014). Examining the deep ocean test stations (Table 4), we find that most of the models have roughly comparable high quality. Sometimes the RMS for GOT5.5 is slightly better than its prior FES2014, sometimes slightly worse (but recall that FES2014 was fit to *all* 151 of these stations, so its RMS values are purely a function of its internal data weighting). The exceptions where improvement is clearly evident are J_1, where the RMS dropped from 0.450 cm to 0.105 cm, and the two quarter-diurnal tides, M_4 and MS_4, where the RMS dropped from 0.120 and 0.128 cm to 0.041 and 0.052 cm, respectively. According to Lyard et al. (2021), the J_1 and MS_4 waves in FES2014 were purely hydrodynamic solutions without data assimilation, and that surely explains much of the GOT5 improvement. In Table 4 both FES2014 and GOT5 show significant improvement over GOT4.7 and EOT20 for M_2, S_2, and S_1 and some improvement for other constituents as well. As seen earlier in Table 3, GOT5.1 and GOT5.5 are usually comparable, except for S_1 where the DAC errors have caused GOT5.5 RMS to exceed GOT5.1: 0.293 versus 0.277 cm; the latter value is lower than all other models, which perhaps can be attributed to its avoidance of the DAC.

For the shelf and coastal tests, Tables 5–6, the most obvious point is the high RMS values for GOT4.7, especially its inordinately high coastal M_2 value. In its (my?) defense, however, with a spatial resolution of 0.5°, it was never intended for use in near-coastal waters. Its performance for shelf stations is more acceptable even if still poorer than that of all the other tabulated models.

GOT5.5 obtains generally the lowest RMS for the shelf stations, but the coastal stations are a trade-off among GOT5.5, FES2014, and EOT20. The latter has the lowest RMS for M_4 and nearly the lowest for several other tides.

In summary, these comparison tables show that GOT5 represents a good advance over GOT4, especially in the shallower waters near coastlines, but also even in the deep ocean (where the M_2 RMS improved from 0.510 cm to 0.307 cm). These tests also highlight the remaining DAC issue, since GOT5.1 appears better than GOT5.5 for S_1 in both deep and coastal waters.

7.2 Ross Ice Shelf

I have done no extensive testing in polar regions, with one exception: the tides under the Ross Ice Shelf, which builds on previous efforts to enlarge the number of *in situ* tide measurements in this remote region (Ray et al., 2021). The *in situ* tide data for the Ross Ice Shelf have always been sparse and mostly based on very short time series, but the situation is slowly improving. The test data employed here are shown in Figure 19. There are two long-term tide gauges operating near the ice shelf at Scott Base and at Cape Roberts; data from both[6] were reanalyzed and extensively discussed elsewhere[7] (Ray et al., 2021).

For many years the only substantial tide measurements over the interior of the ice shelf were from a set of eight gravity stations deployed across the whole shelf. The gravimetric tides were analyzed and reported by Williams & Robinson (1980). This gravity campaign established that the Ross Ice Shelf tides were primarily diurnal—confirming and extending older observations made

[6]I thank Glen Rowe of LINZ, New Zealand, for the Cape Roberts hourly data. The Scott Base data were downloaded from the University of Hawaii sea level archives; the data originated from NIWA, New Zealand.

[7]The reanalyzed tide gauge results supplant previous publications based on shorter time series (e.g., Goring & Pyne, 2003), and not only because longer time series normally result in smaller uncertainties. It turns out that both stations observe degree-3 semidiurnal tides that are fairly large (i.e., large for degree-3 tides), almost 5 mm for $^3N_2$. These will corrupt estimates of the usual, degree-2, N_2 if the time series is much shorter than 8 years.

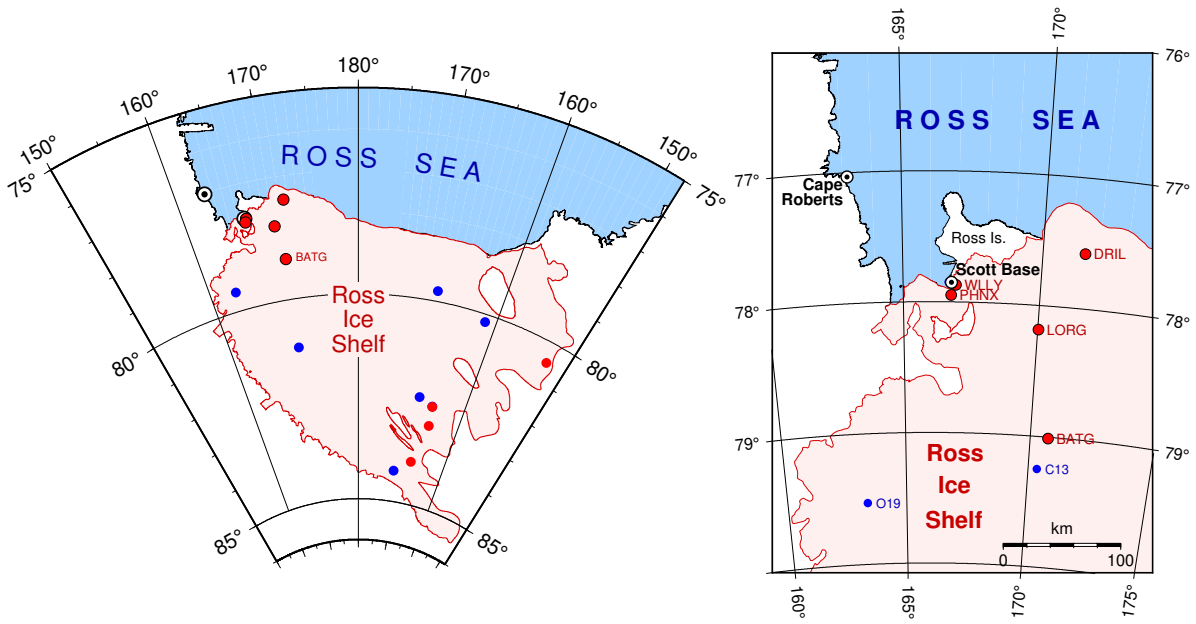

Figure 19: Tide gauge stations on or near the Ross Ice Shelf. Blue dots are gravimeter stations reported by Williams & Robinson (1980). Red dots are GPS stations: short time series in the southeast from the AntTG database, longer time series in the northwest from Ray et al. (2021). Right panel is a zoom view of the northwest, showing the newer GPS stations as well as the two long-term tide gauges at Scott Base and Cape Roberts.

near Ross Island—and that the semidiurnal waves had amphidromes either under the ice shelf or near it. The time series were all understandably short, between 29 and 58 days, and difficult to make in light of the moving gravimeter platform (i.e., the flexing ice). Harmonic constants for six of these gravimeter stations, extracted from Table 2 of Williams & Robinson (1980), are used here for testing.[8]

The gravimeter stations have been supplemented in recent years by GNSS stations (actually only GPS so far) sitting on the floating ice. Tidal estimates from four short GPS time series have been extracted from the AntTG database (maintained primarily by Laurie Padman and Susan Howard; see `https://doi.org/10.15784/601358`). Available documentation is minimal for these four sites, aside from the lengths of the time series, which were all short: between 43 and 78 days.

I also use five newer GPS-based tide estimates, located on the northwest part of the ice shelf. These are all based on much longer time series, more than two years except for one station (LORG) of 289 days. Harmonic constants are given in a supplement to Ray et al. (2021).

GPS-based tide estimates require correction for vertical displacements caused by solid tides. The body tide is no problem, but the load tide is, as all existing ocean-tide models in this region

[8]Tidal constants for the gravimeter stations are slightly different in the AntTG database, having been adjusted for reasons unclear to me. Moreover, two of the stations have been here discarded: stations C13 and J9. As discussed in more detail elsewhere (Ray et al., 2021), gravity station C13 is suspect: its O_1 amplitude appears too large, 4 cm larger than its K_1, which is not consistent with tidal characteristics of the region. Moreover, C13 is near GPS station BATG (see right panel of Figure 19), which has a much longer and more reliable dataset, and its tidal constants disagree with those from C13. Gravity station J9 is almost exactly at the same location as GPS station RIS-BFLT, and it is not far from gravity station BASE. The K_1 amplitudes for these three stations are 43 cm, 37 cm, and 42 cm, with J1 being the low one, by an unacceptably large amount. Thus, station J1 is discarded.

must be treated with caution. The new GPS data (Ray et al., 2021) were adjusted during the original GPS data processing by using the FES2004 load tides. Errors in that model could potentially induce errors in the GPS-based constants for O_1 and K_1 of as much as 1 cm. Eventually, any GPS data in this region requires an iterative reprocessing, as models of ocean tides improve. The load-tide model used for the older GPS stations is unknown.

It is interesting to examine how GOT5.5 compares against each of these four sets of harmonic constants. For the three main constituents, the RMS differences in cm are:

	O_1	K_1	M_2
Scott & Cape Robert tide gauges	1.13	1.66	1.41
Five new GPS stations	1.20	2.80	1.40
Four old GPS stations	3.93	3.59	2.07
Six old gravity stations	3.49	2.34	3.30

Assuming that GOT5.5 errors are of comparable magnitude across the entire shelf (an admittedly dubious assumption), this table indicates that the two tide gauges and the five new GPS stations are more accurate than the older stations, except for K_1. This is reasonable in light of the short time series of the older data. All GPS stations see relatively large differences for K_1. This could be due to the high sensitivity that K_1 GPS estimates have to any orbit error and/or multipath errors (e.g., King, 2006). Or it could be due to larger errors in GOT5.5 at K_1 because of its dependence solely on CryoSat-2 data.

Notwithstanding these qualifications about data quality, I have combined all 17 *in situ* stations and computed RMS differences with GOT5.5 and FES2014 (to my knowledge, FES2014 did not assimilate any of these data). These comparisons were done for only constituents K_1, O_1, M_2, and S_2. The 10 older stations, both gravimeter and GPS, are all too short to separate P_1 from K_1 or K_2 from S_2, and the gravity stations reported no estimates for Q_1. Results are given in Table 7. Relative to the prior FES2014, the two large diurnal tides see good improvement. However, the GOT5 solution for the small M_2 has degraded the prior. No one station explains this degradation. Both GOT5 and FES2014 observe largest M_2 discrepancies for the two gravity stations BASE and F9. In contrast, both GOT5 and FES2014 differences for S_2 are dominated by poor agreement with the four old GPS stations in the southeast and especially poor agreement with GPS station RIS-DFLT. I suspect the tidal analysis at that station is flawed; the series is only 74 days long, too short (as noted above) to separate S_2 and K_2, and yet the AntTG database reports S_2 and K_2 amplitudes of 14 and 10 cm, respectively, which is a suspiciously large K_2-to-S_2 ratio.

Table 7: RMS differences (cm) with 17 Ross Ice Shelf stations.

	O_1	K_1	M_2	S_2
FES2014	6.37	4.93	2.05	2.96
GOT5.5	2.92	2.76	2.28	2.74

8 Tide Prediction Package perth5

To use the GOT5 files of tidal amplitudes and phases to predict tidal elevations an updated set of prediction codes has been witten. The new package, written in a (mostly) modernized Fortran, is more powerful and flexible than my previous codes released with, for example, GOT4 data.

The code, dubbed perth5 is a user-callable module designed to compute tidal heights for a desired time and location. It uses as input the two-dimensional GOT5 grids, but it can handle a number of other tide formats (ascii, netcdf, and the native binary from the Oregon State model), and it can handle any number of constituents. On option it can use tidal inference for any missing (diurnal or semidiurnal) waves, using either linear or Fourier-series interpolation/extrapolation of tidal admittances. The input grids must store one constituent in each input file, which is currently the most common approach.

The package is under git version control; see https://codeberg.org/rray/perth5.

The CNES FES tide models come with their own prediction software, written mostly in C. By design, perth5 can also handle the FES model netcdf files. (It cannot at this point handle the FES finite-element files.) A package comparable to perth5 has been written in python by Tyler Sutterley; see https://github.com/tsutterley/pyTMD.

Further documentation for perth5 consists of comments at the beginning of the module:

```
module perth

!  Module for the perth5 tide prediction code

!  Purpose: to compute the ocean tide height at a given time and location
!  from grids of harmonic constants.  An arbitary number of grids may be
!  input, with each grid containing the constants for one constituent.
!  Several grid formats can be handled.
!  This routine requires linking to a netCDF library.

!  The main user-callable subroutine is perth5, whose calling arguments are
!  the same as older versions of the "perth" software used for GOT models.
!
!           SUBROUTINE PERTH5( DLAT, DLON, TIME, TIDE, ISDATA )
!  where:
!    DLAT,DLON - latitude and longitude in degrees for desired location.
!             - can be Y,X if input grids use a cartesian coordinate system.
!    TIME - desired UT time, in decimal Modified Julian Date.
!    TIDE - the computed tidal height, in same units as input amplitude grids.
!    ISDATA - logical denoting whether tide data exist at the desired location
!
!  Before the PERTH5 subroutine is called, an initialization subroutine must
!  be called.  It has some optional arguments, although the defaults should be
!  taken for most purposes.  All arguments are input, none are output.
!
!      SUBROUTINE PERTH5_INITIALIZE( DATASETNAME, NDATASETS, INPUT_FORMAT, &
```

```
!               VERBOSE, NODAL_CORRS, INFERENCE )
!  where:
!     DATASETNAME - an array of file names, each file holding one constituent
!          (unless INPUT_FORMAT=0 in which case all constituents are in one file).
!     NDATASETS - number of files to read (= length of array DATASETNAME).
!     INPUT_FORMAT - format of input grid files:
!         = 1 for ascii grids used for the GOT4 (and earlier) tide models.
!         = 2 for binary (big-endian) OTIS grids used for the TPXO tide models.
!         = 3 for models given in generic netcdf files  [default].
!         = 4 for netCDF grids used for FES2014 tide model.  Now same as = 3.
!         = 0 for NO grid, but rather for one file holding a list of tidal constants
!             for a single location. (In this case, PERTH5 will ignore DLAT,DLON.)
!             The file must hold ascii columns with: tide name, amplitude, phase lag,
!             plus an initial record giving the number of tidal constants to be read.
!             Look in subroutine doodno8 for allowed tide names.)
!     VERBOSE - 0, 1, 2, or 3 controls amount of printout. 0 = none [default].
!     NODAL_CORRS - optional integer denoting whether to apply nodal corrections.
!         = 0 for none;  1 = yes [default];
!         = 2, computes group modulations [use only if you know what you're doing].
!     INFERENCE - optional integer denoting whether to infer minor diurnal/semid'l
!           constituents that are not input as grids.  [default = 1].
!         = 0, no inference is done; only input constituents are used for prediction.
!         = 1, inference is done by piecewise linear interpolation of admittances.
!         = 2, inference is done by Munk-Cartwright Fourier interpolation.
!       The software determines which constituents may be inferred.  However,
!       inference requires at least 6 constituents as input: Q1,O1,K1,N2,M2,S2.
!       This routine will accept long-period tides, if input, but it will not infer
!       any missing ones; use perth_lp module for that.
!       The routine makes a valiant attempt to recognize the constituent
!       names that reside in the input grids; contact me if it fails.
!
```

9 Atlas of Cotidal Charts

The following atlas of global charts includes all twenty constituents estimated as part of GOT5.5 and GOT5.6, including four degree-3 constituents (the names of the latter include a leading superscript '3'). Inferred constituents are not included even though a number of these are in the distributed GOT5 tar files. (Those extra inferred tides are in the tar files as a courtesy to users with certain applications—e.g., GEODYN users—but the inferred tides are not needed for tide prediction if using the supplied `perth5` package.)

As these are empirically derived maps, they are subject to measurement noise—unlike maps from numerical models. Some slight cosmetic smoothing has been applied to smaller constituents, although phase lines can still be somewhat erratic where amplitudes are very small.

On most of the charts, Greenwich phase lines are plotted in white every 30°, with thicker white lines marking the 0° isolines; small arrows on the thicker lines give the sense of direction of wave propagation. For some constituents with small amplitudes where phases are noisy, the phase contours are every 60°. The two quarter-diurnal compound tides are very small in the deep ocean except in the Atlantic. In much of the Pacific their phase lines are mostly disorganized and appear to wander around aimlessly—not unexpected when amplitudes are so small.

The following charts are given in order of increasing frequency, from σ_1 to MS_4.

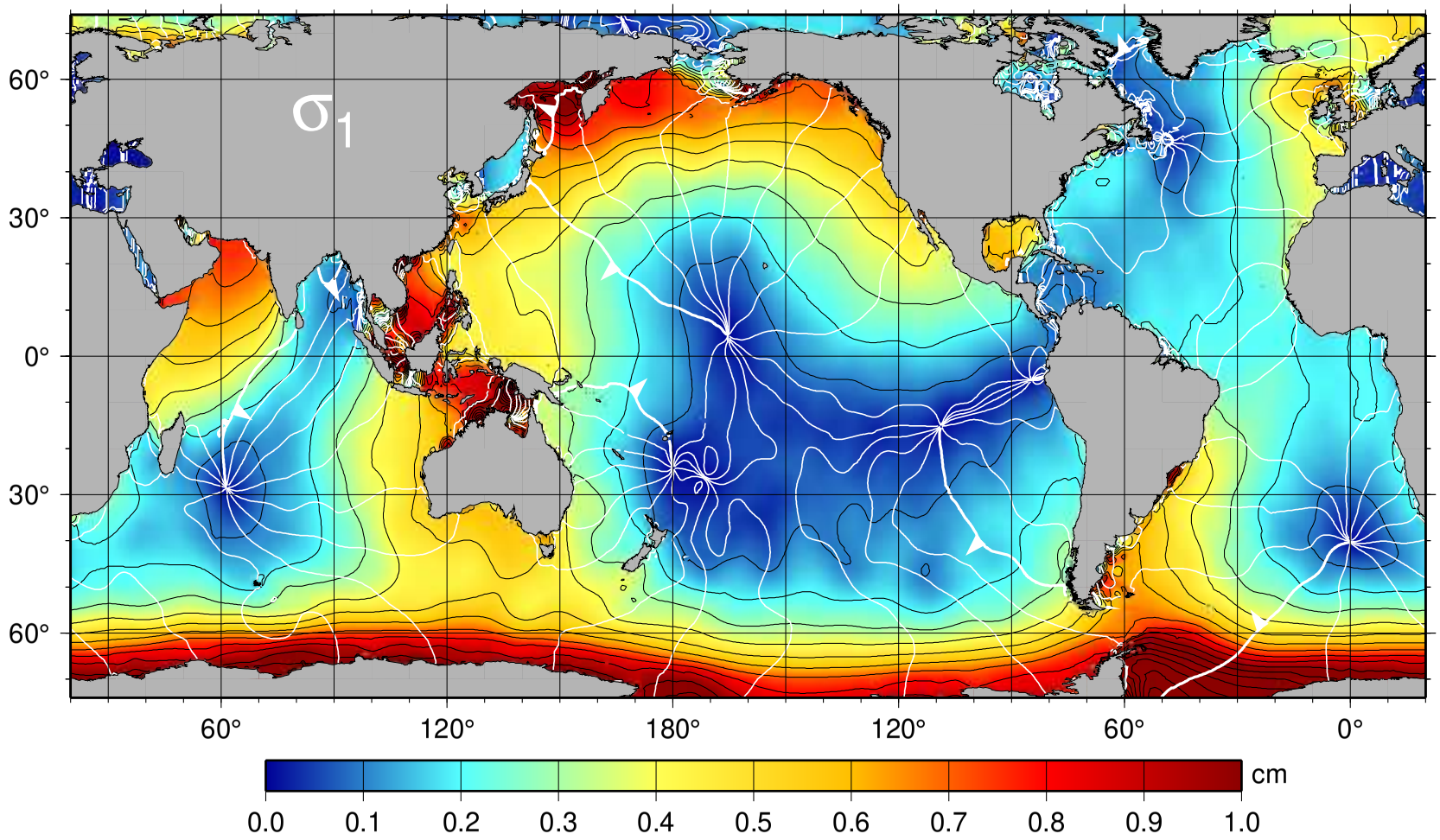

Figure 20: Cotidal chart of constituent σ_1.

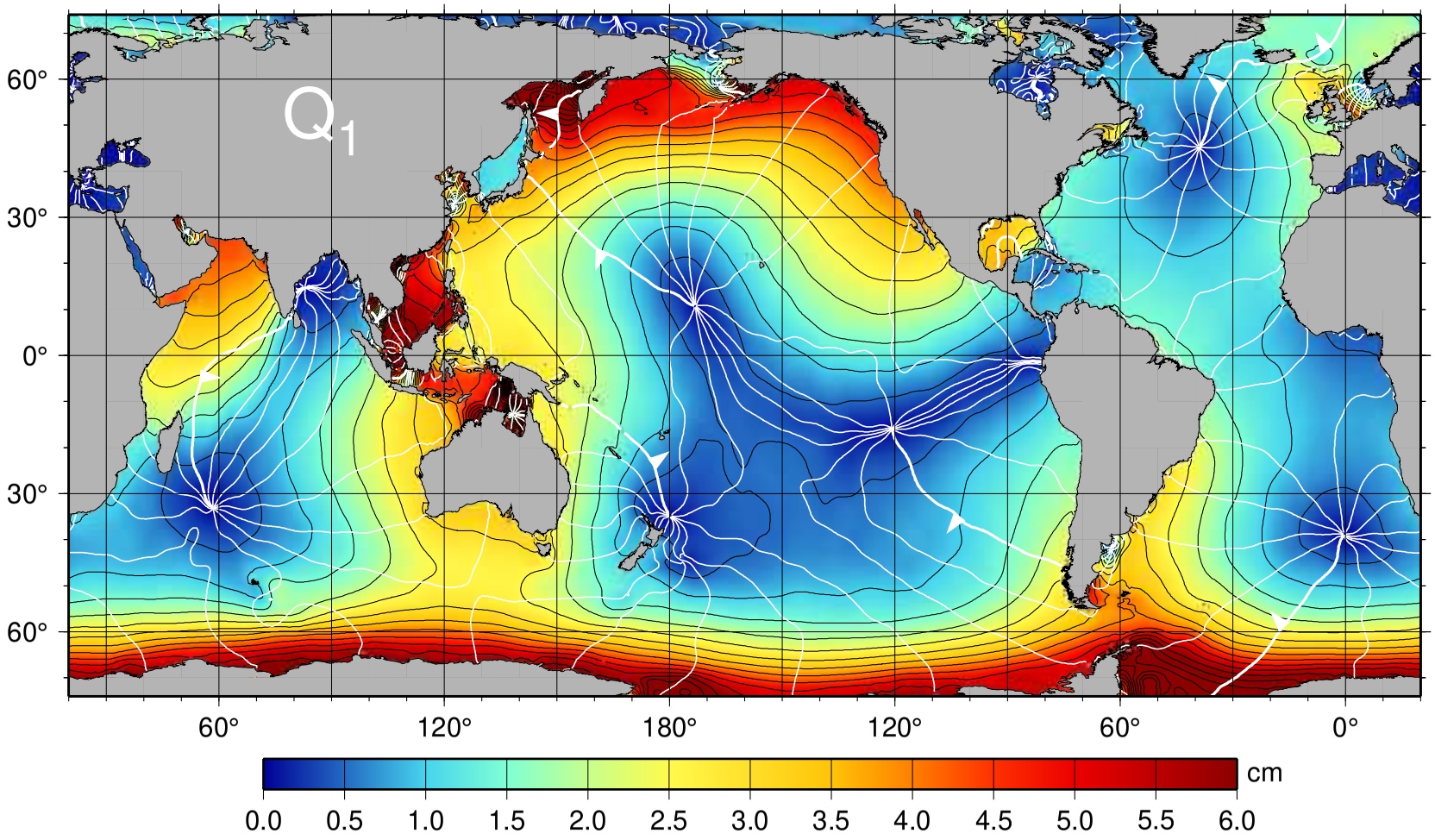

Figure 21: Cotidal chart of constituent Q_1.

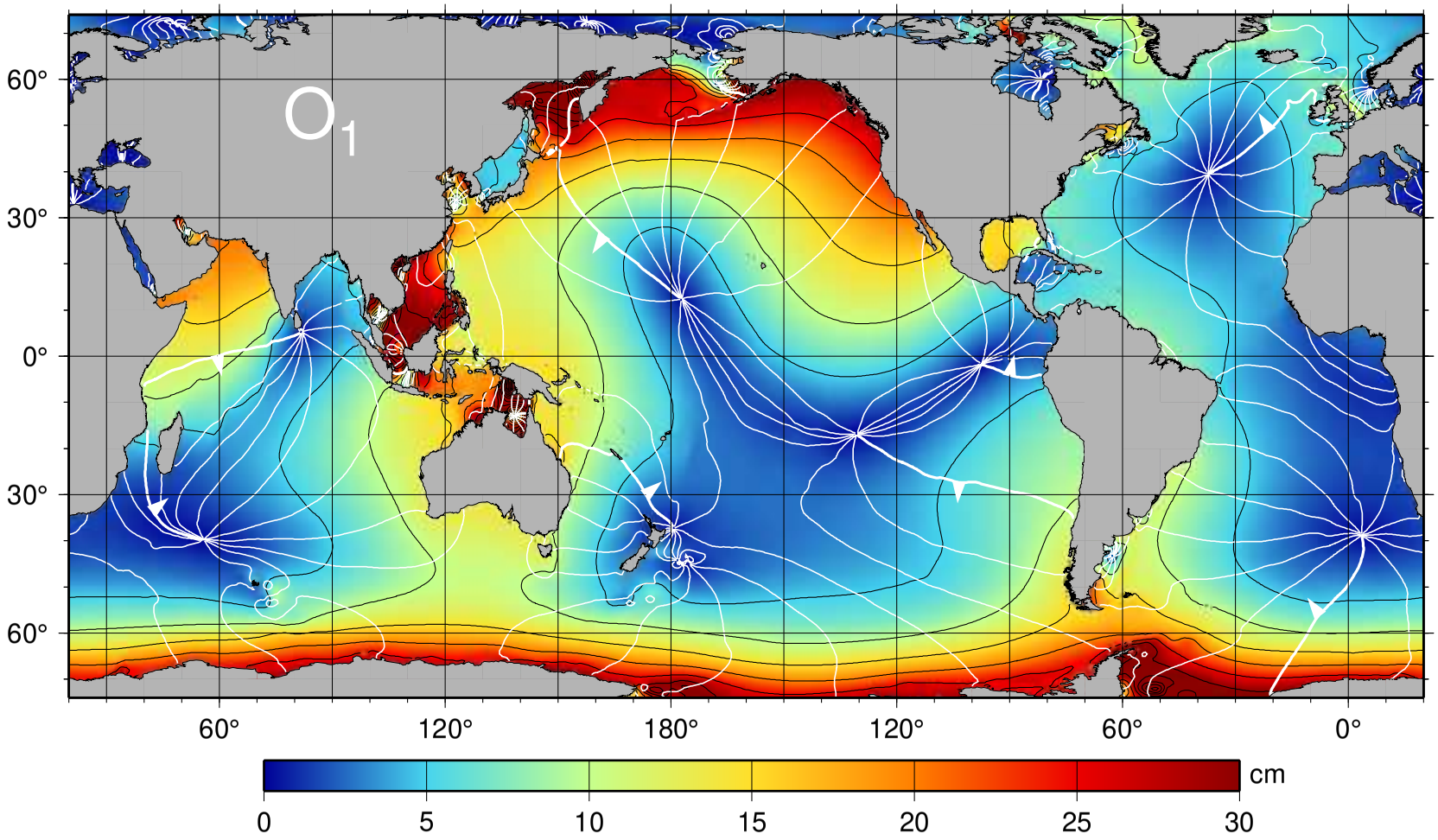

Figure 22: Cotidal chart of constituent O_1.

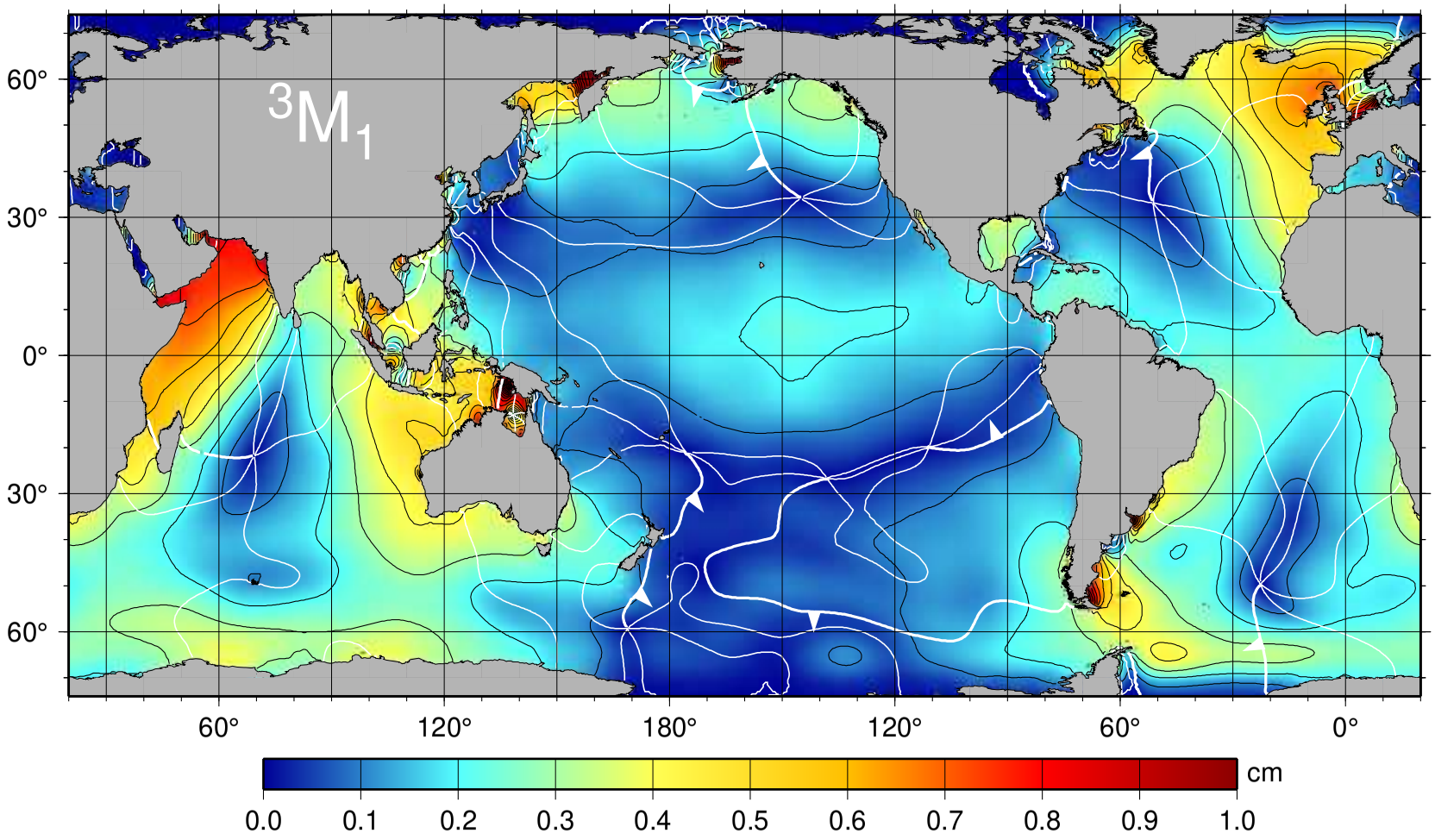

Figure 23: Cotidal chart of constituent $^3M_1$, a constituent generated by the third-degree terms in the tidal potential.

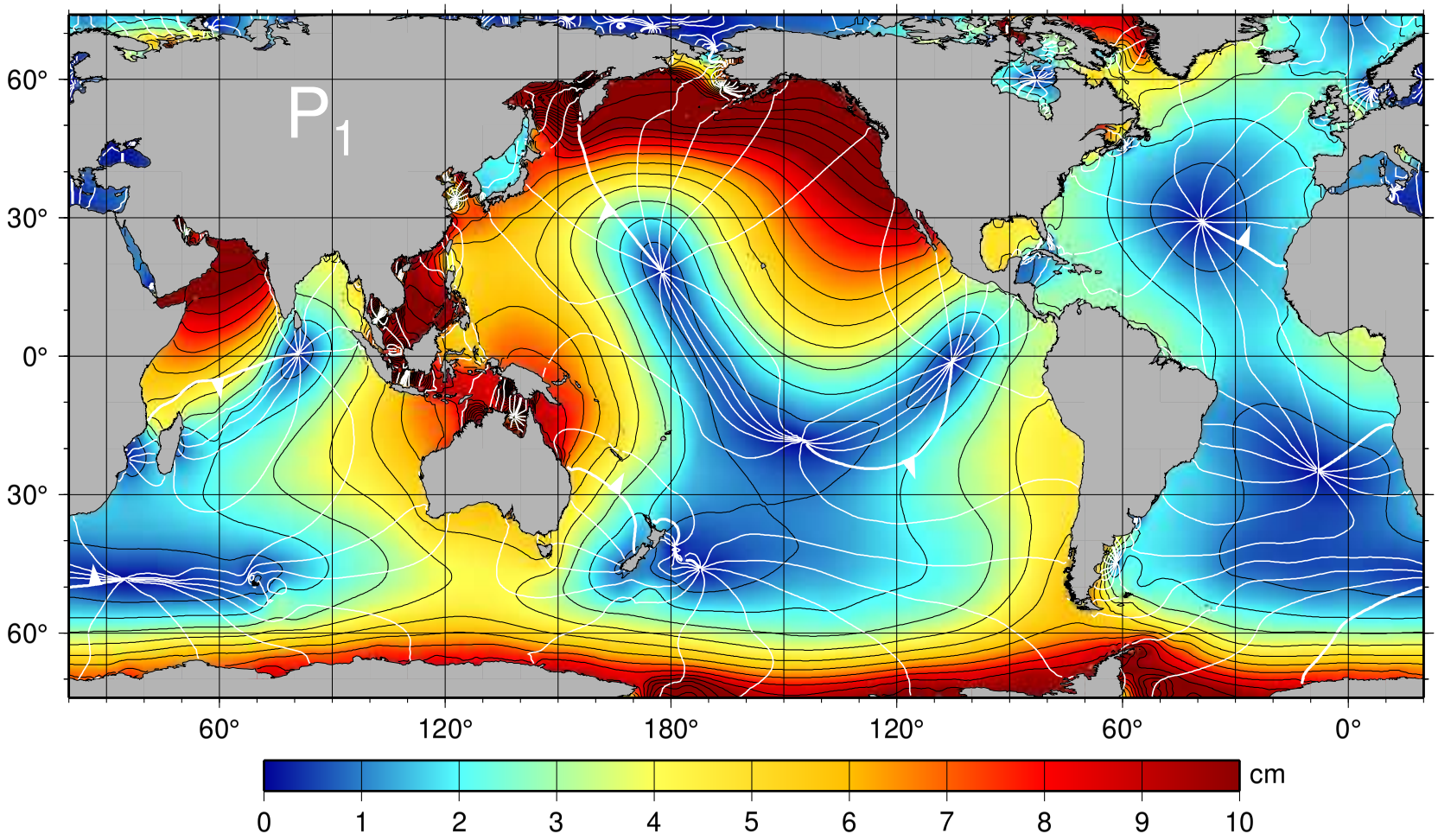

Figure 24: Cotidal chart of constituent P_1.

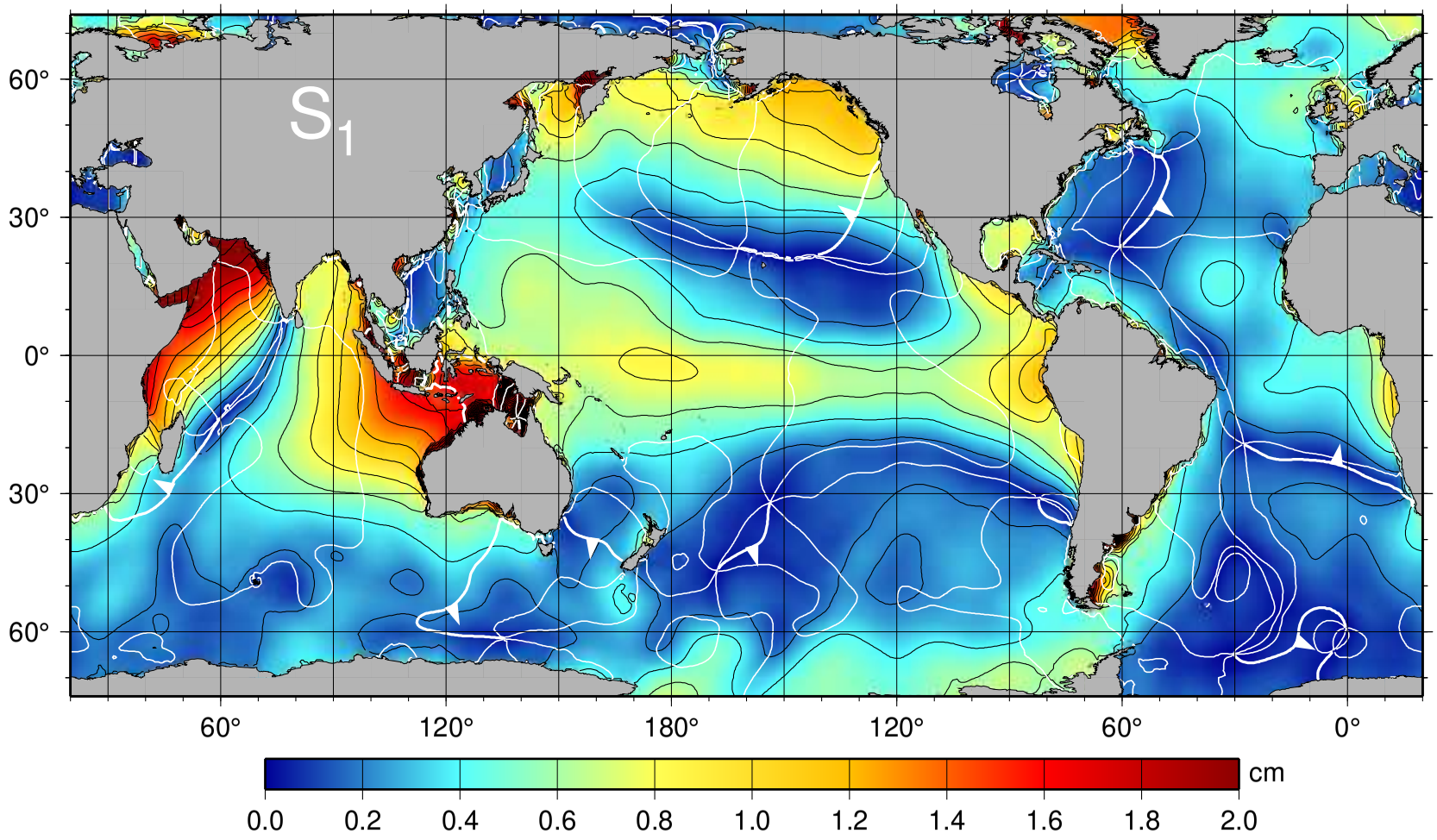

Figure 25: Cotidal chart of constituent S_1.

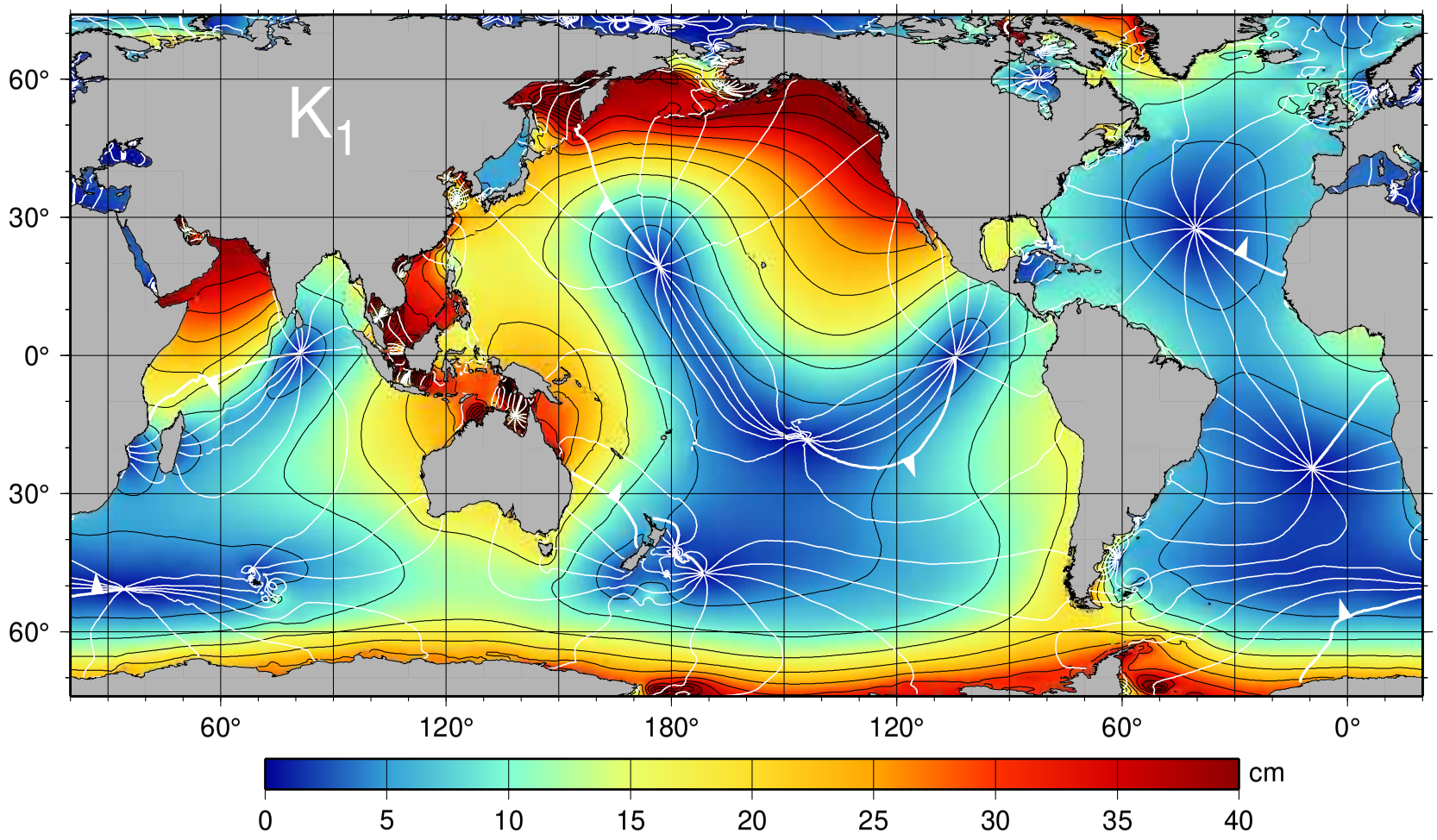

Figure 26: Cotidal chart of constituent K_1.

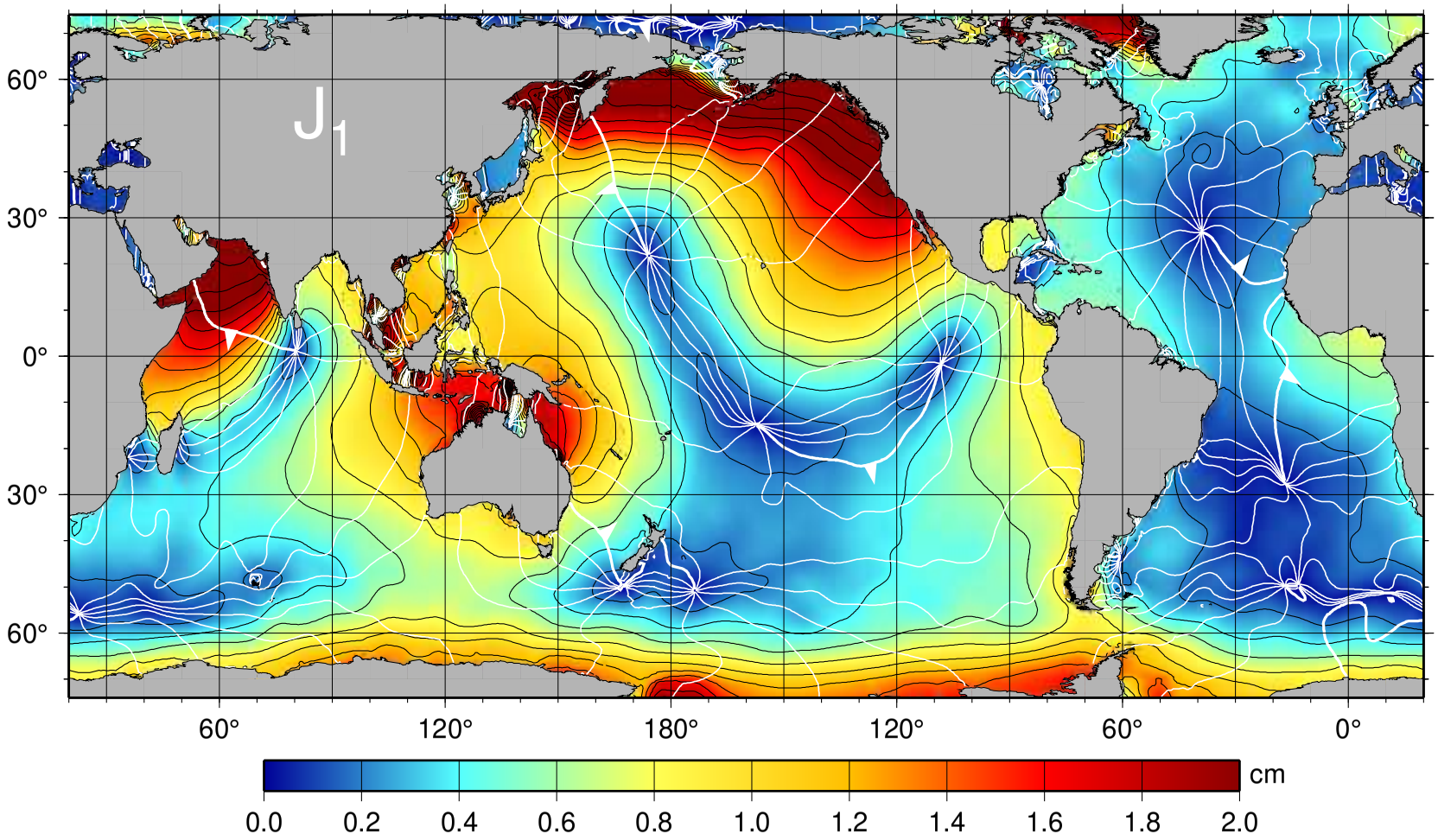

Figure 27: Cotidal chart of constituent J_1.

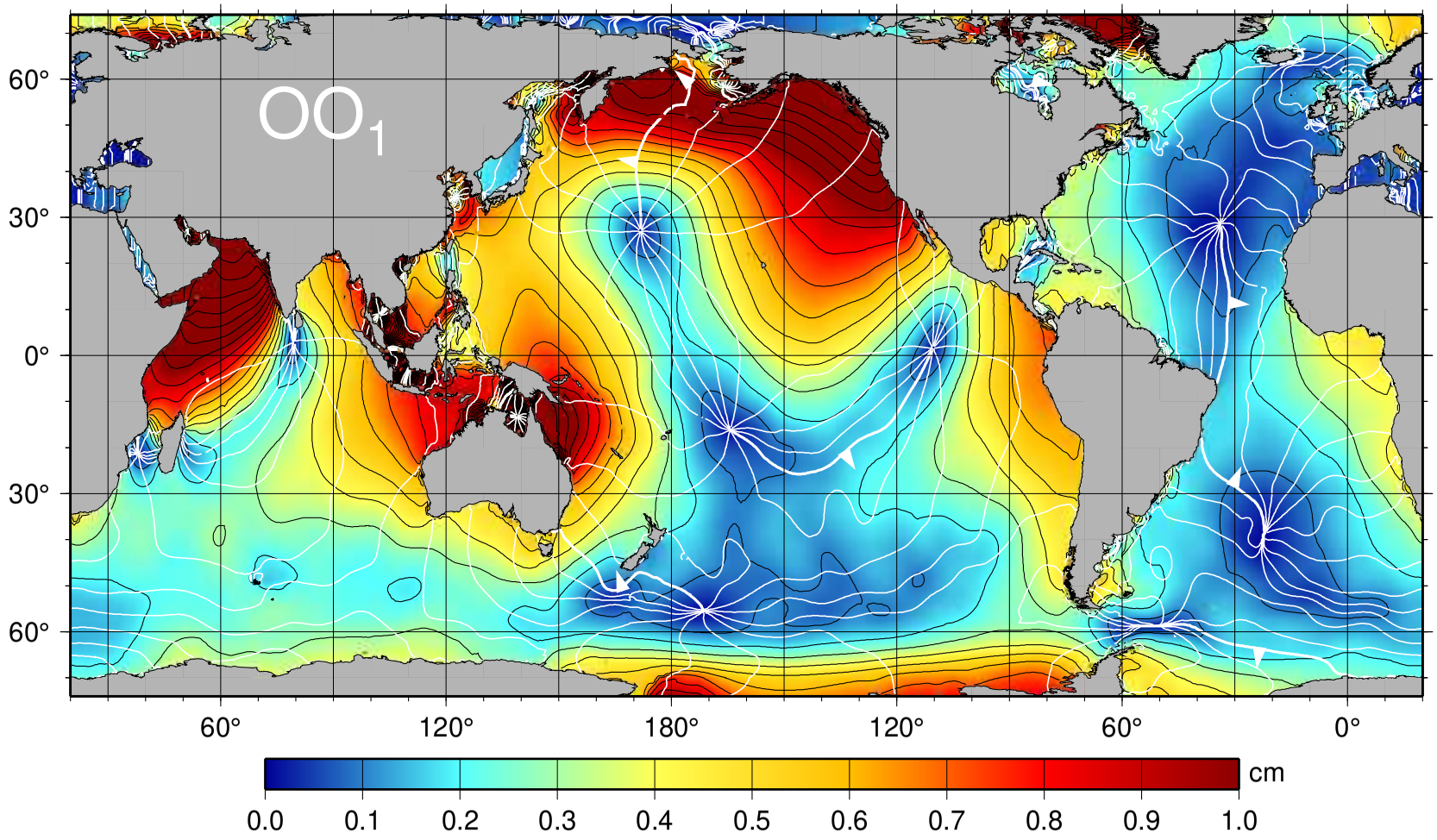

Figure 28: Cotidal chart of constituent OO_1.

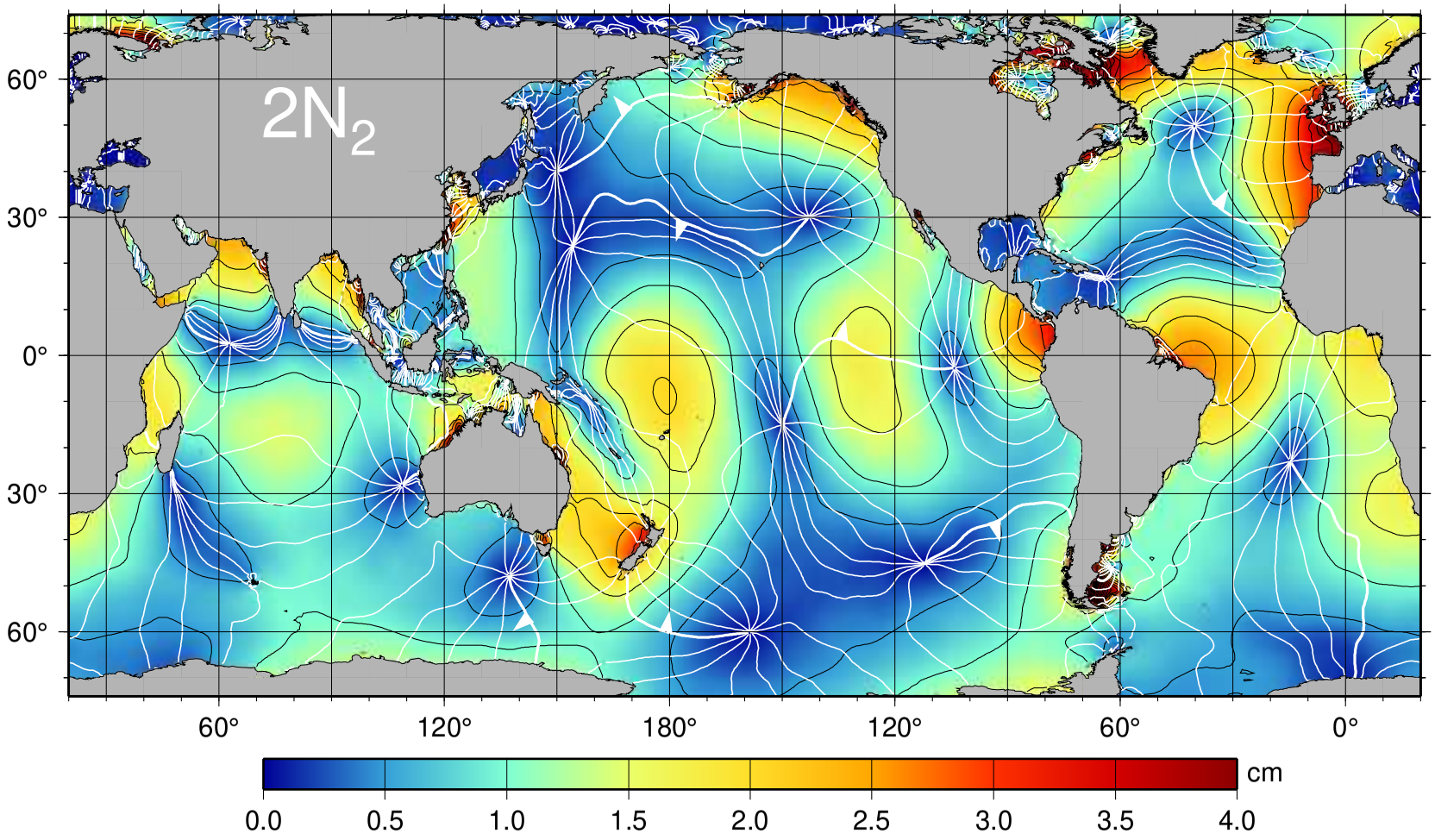

Figure 29: Cotidal chart of constituent $2N_2$.

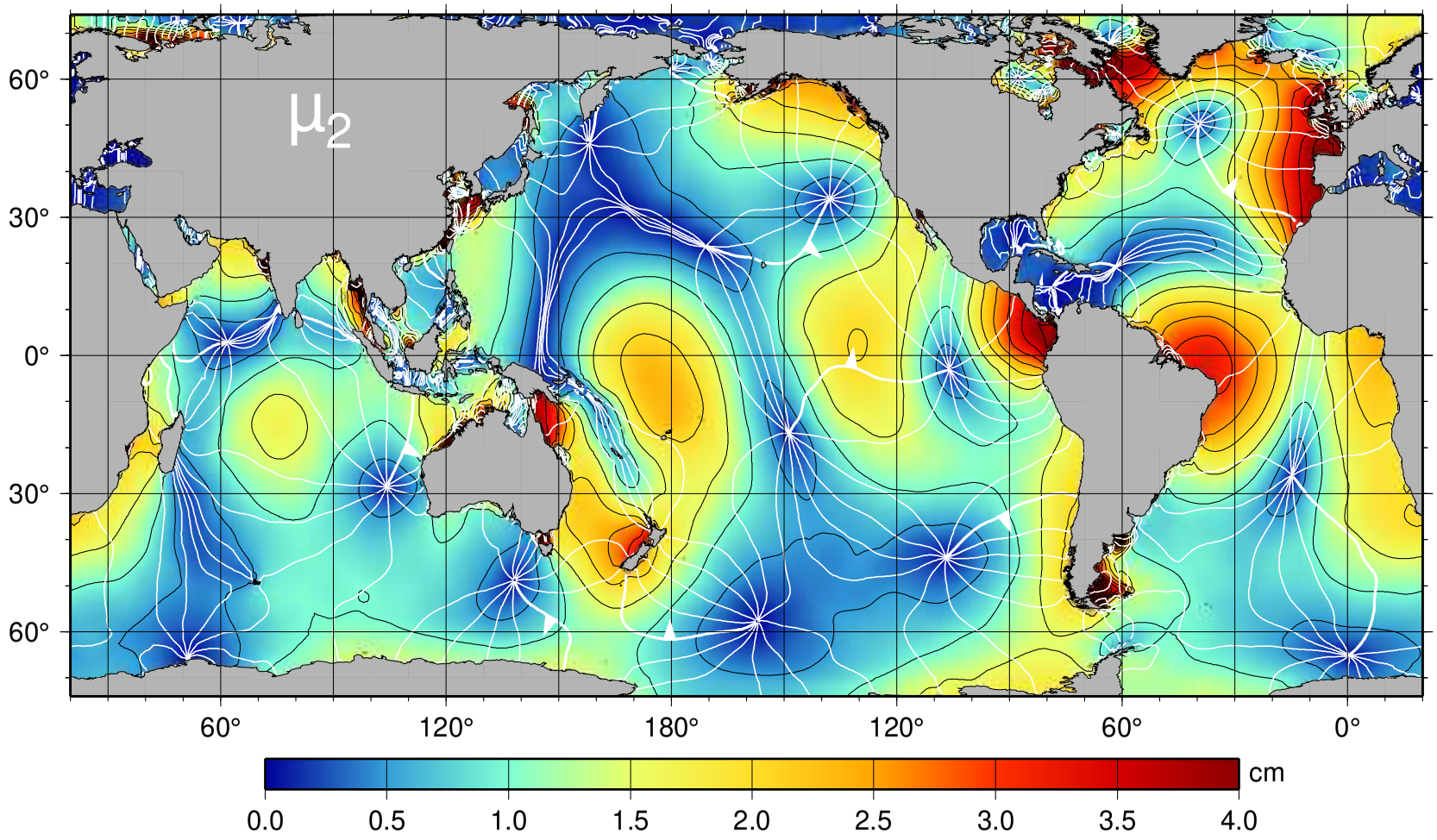

Figure 30: Cotidal chart of constituent μ_2.

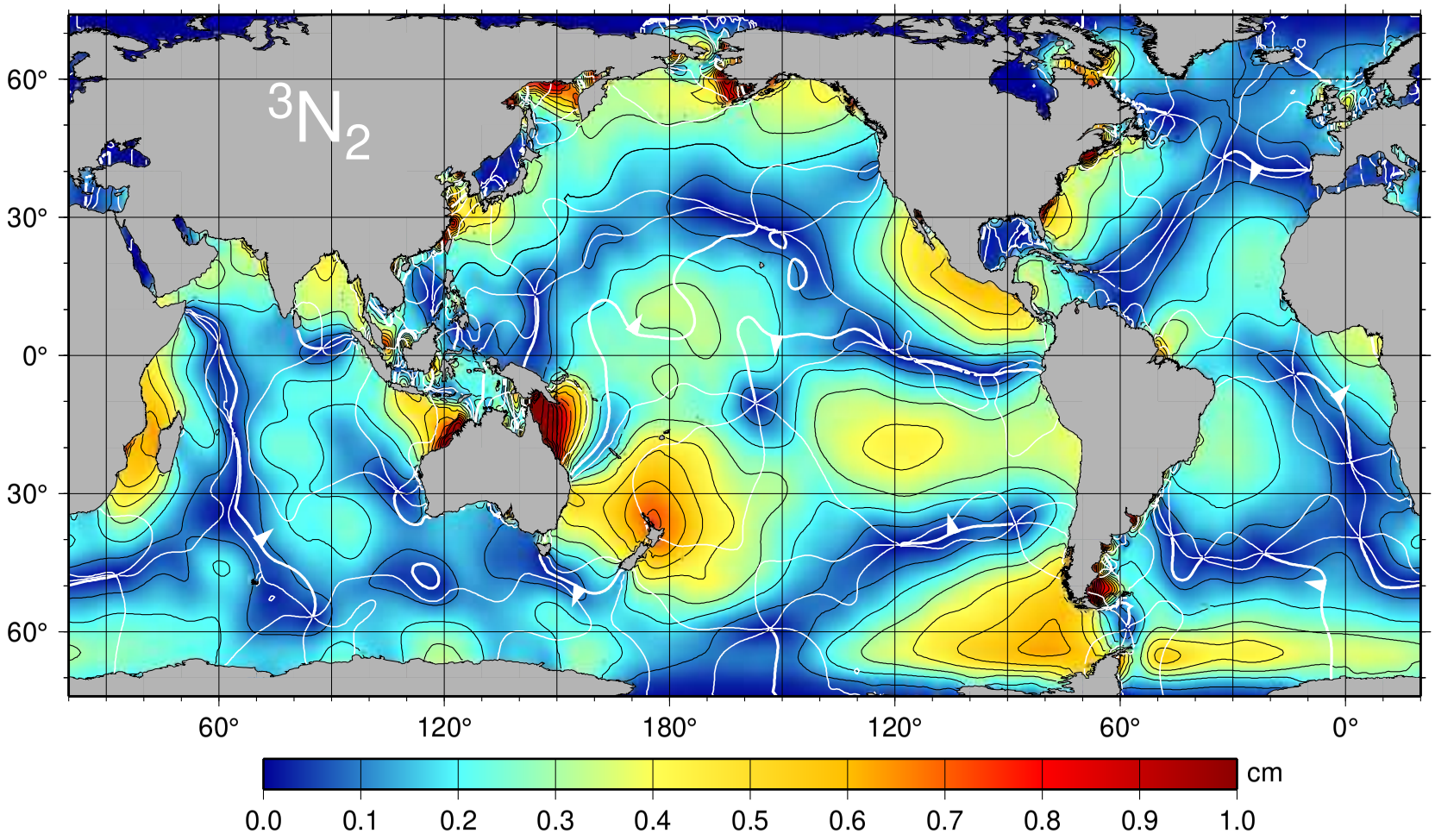

Figure 31: Cotidal chart of constituent $^3N_2$, a constituent generated by the third-degree terms in the tidal potential.

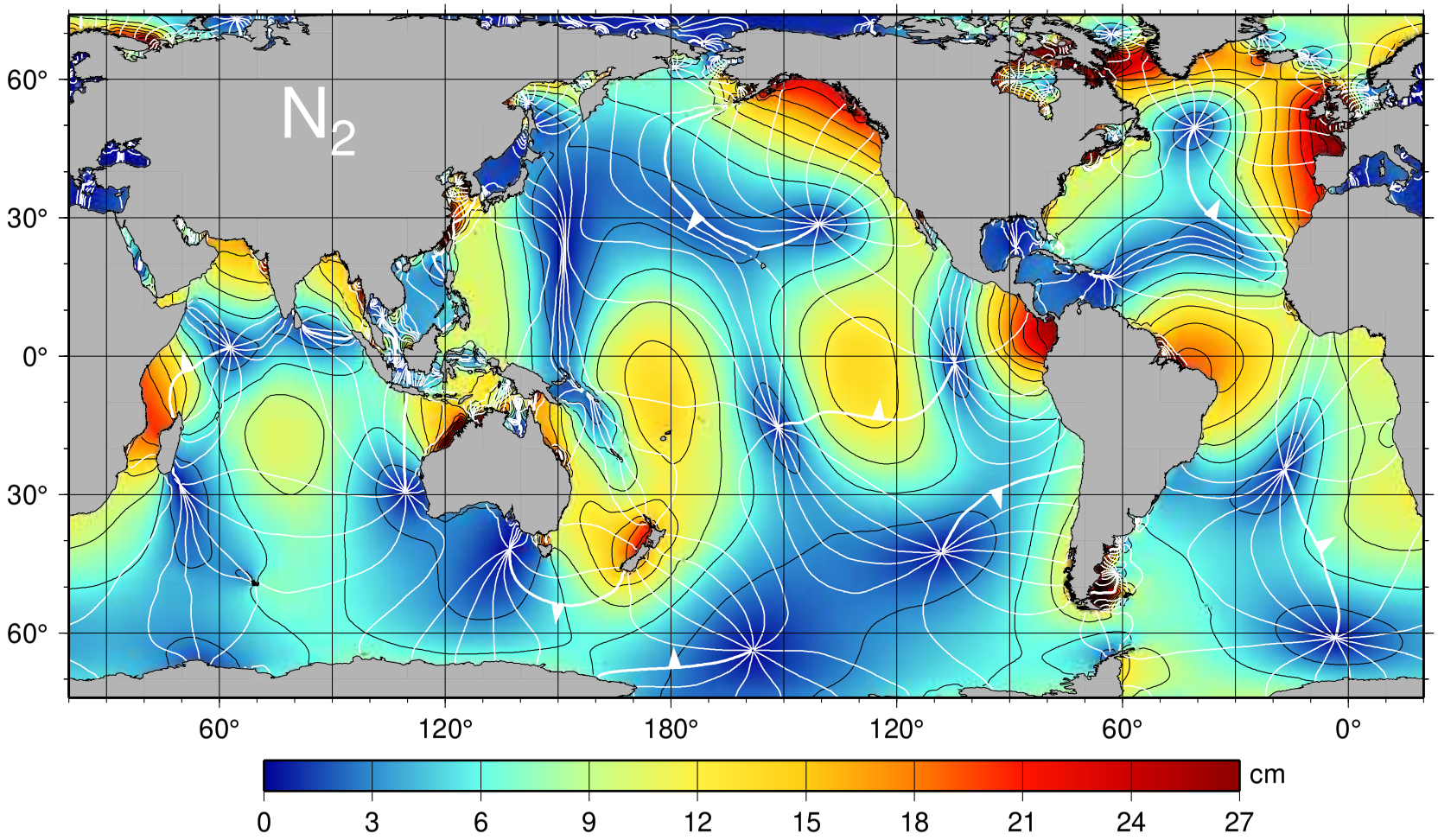

Figure 32: Cotidal chart of constituent N_2.

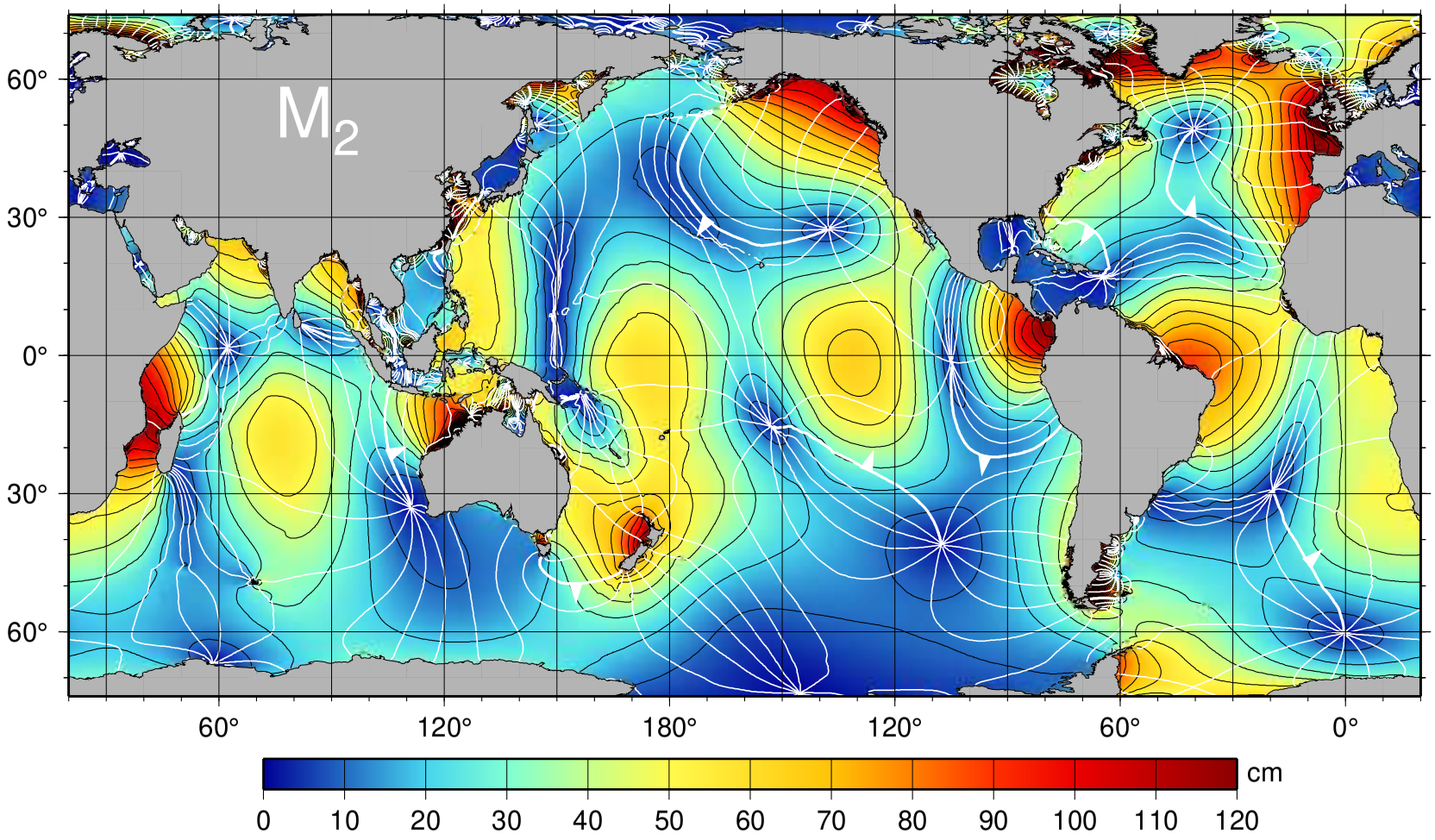

Figure 33: Cotidal chart of constituent M_2.

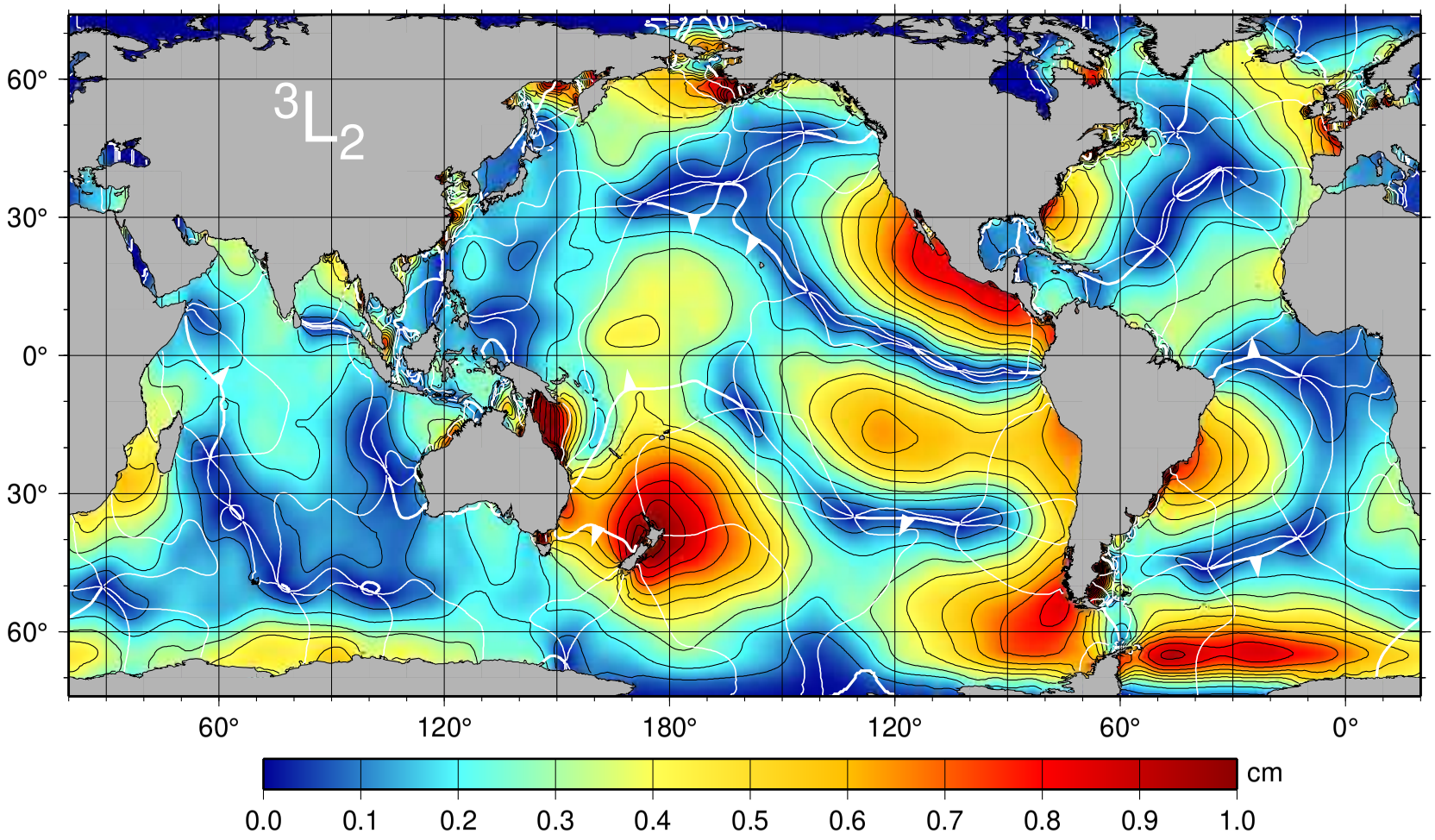

Figure 34: Cotidal chart of constituent $^3L_2$, a constituent generated by the third-degree terms in the tidal potential.

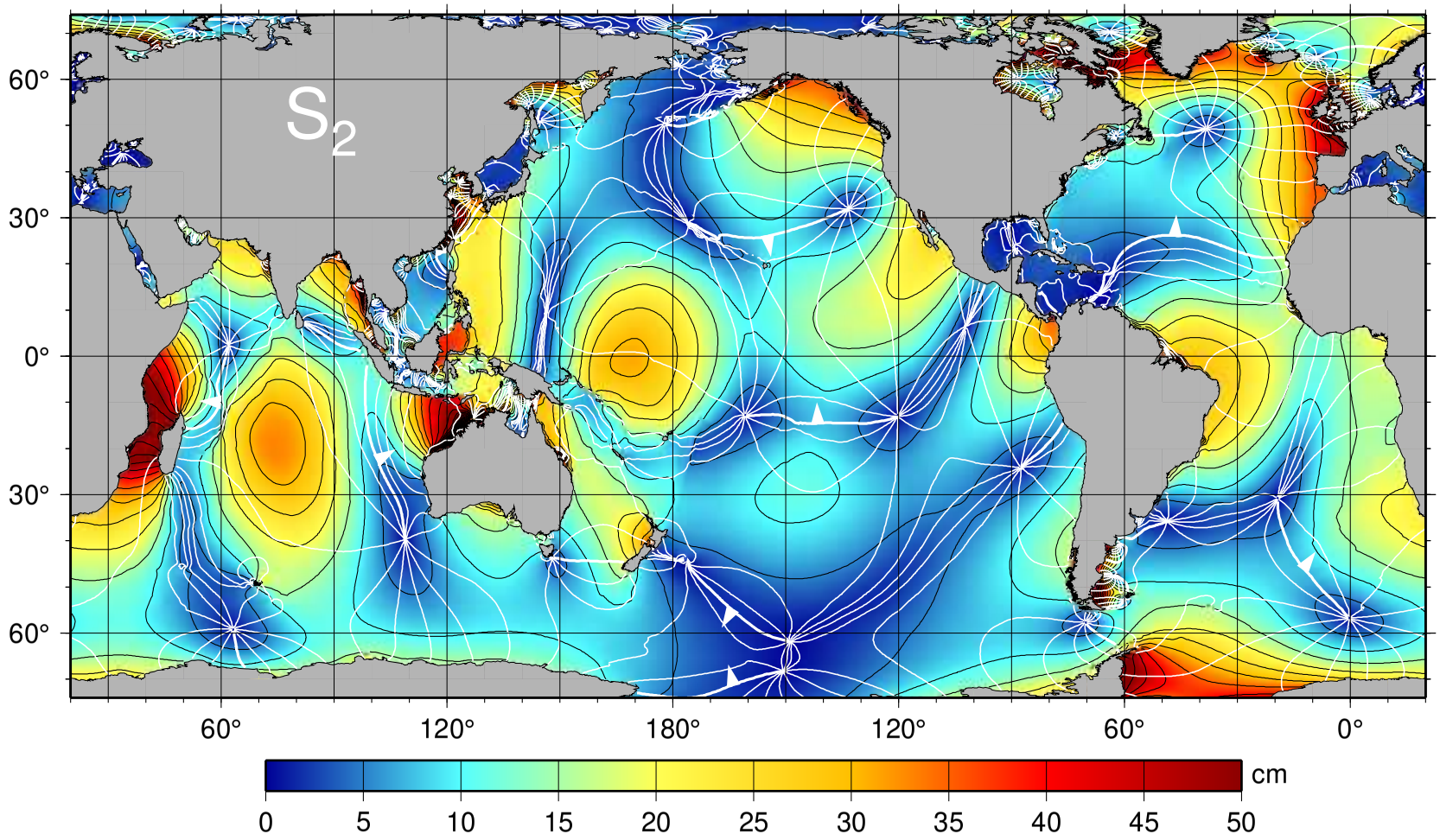

Figure 35: Cotidal chart of constituent S_2.

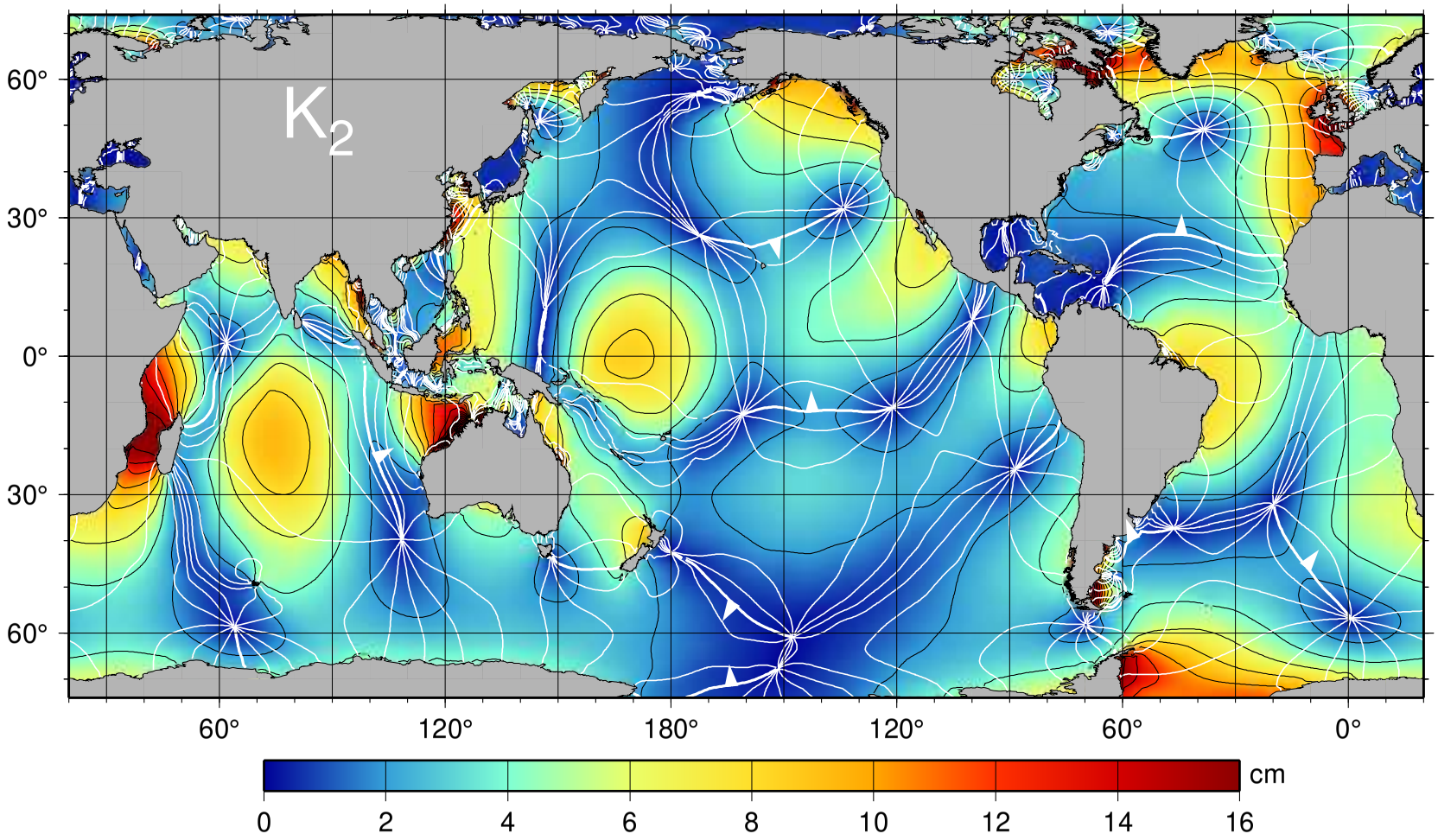

Figure 36: Cotidal chart of constituent K_2.

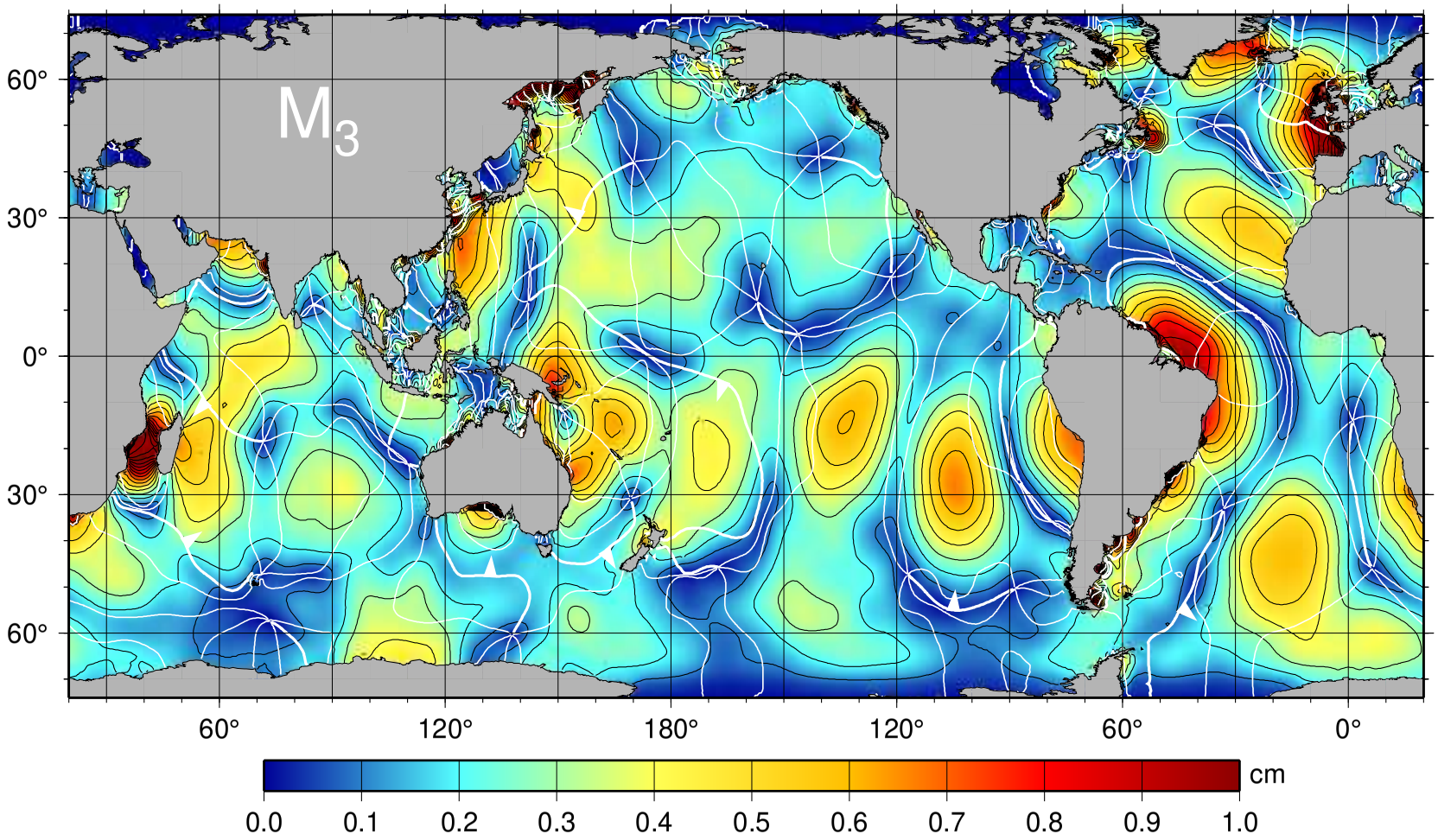

Figure 37: Cotidal chart of constituent M_3.

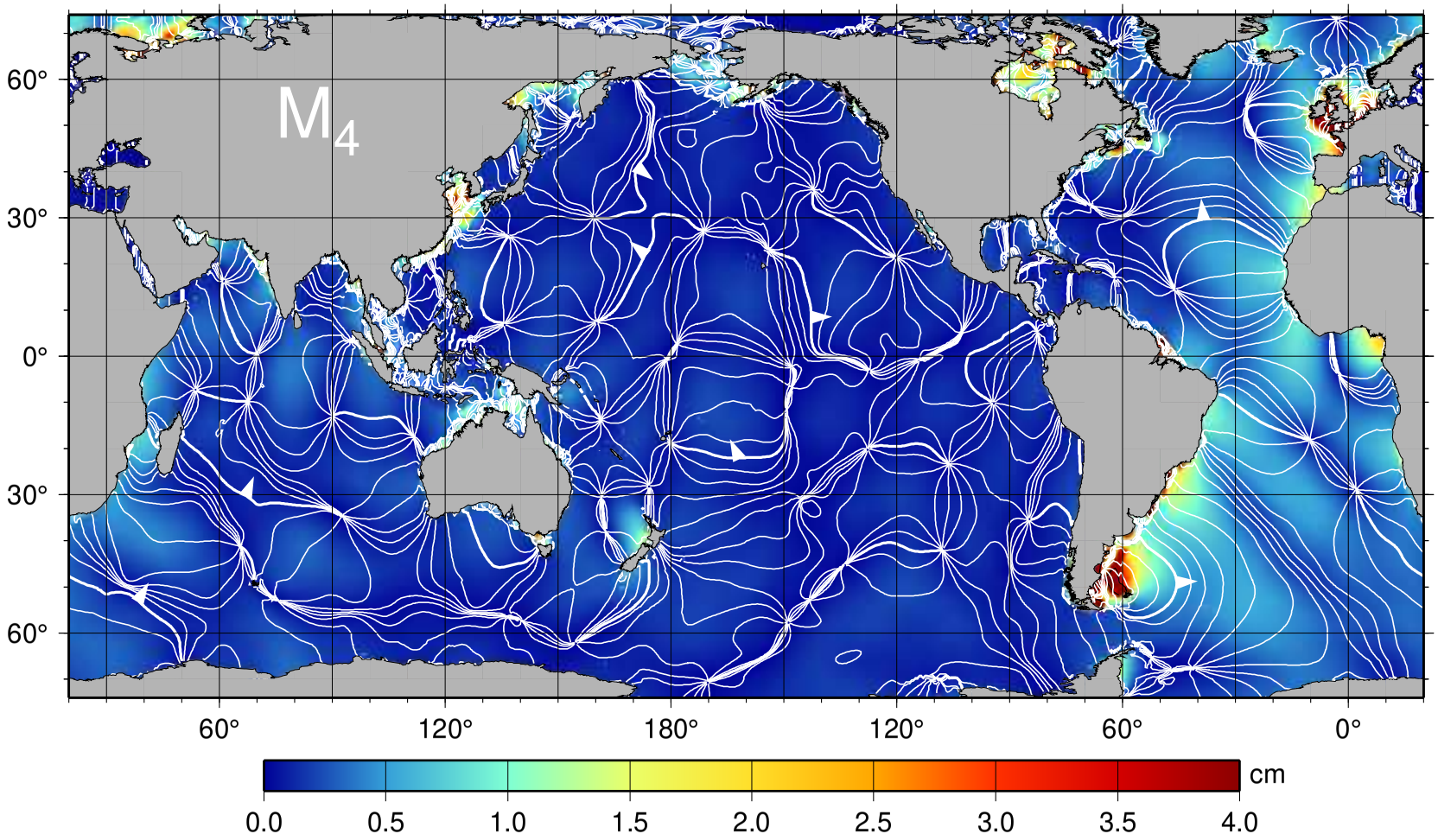

Figure 38: Cotidal chart of constituent M_4, a nonlinear compound tide.

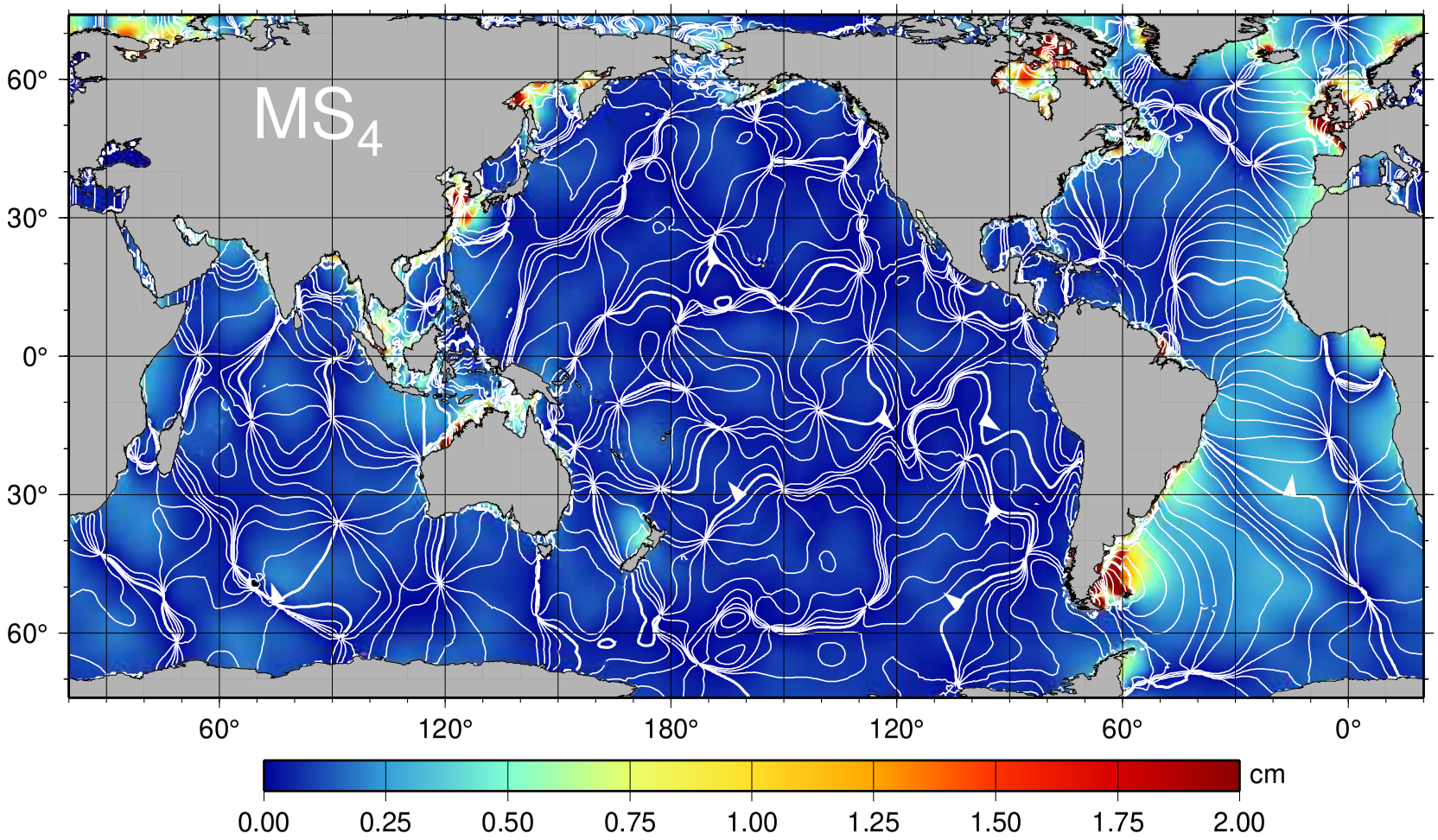

Figure 39: Cotidal chart of constituent MS_4, a nonlinear compound tide.

References

Ablain, M., et al. (2010, October). *Analysis of 58.74-day signal observed on the MSL derived from Jason-1&2 and TOPEX data.* Ocean Surface Topography Science Team meeting, Lisbon. Retrieved from https://www.aviso.altimetry.fr/fileadmin/documents/OSTST/2010/oral/20_Wednesday/morning/Ablain.pdf

Andersen, O. B., Rose, S. K., Abulaitijiang, A., Zhang, S., & Fleury, S. (2023). The DTU21 global mean sea surface and first evaluation. *Earth System Science Data*, *15*, 4065–4075. doi: 10.5194/essd-15-4065-2023

Andersen, O. B., Rose, S. K., & Hart-Davis, M. G. (2023). Polar ocean tides—revisited using Cryosat-2. *Remote Sensing*, *15*, 4479. doi: 10.3390/rs15184479

Arbic, B. K. (2005). Atmospheric forcing of the oceanic semidiurnal tide. *Geophysical Research Letters*, *32*(2), L02610. doi: 10.1029/2004GL021668

Boy, F., Desjonquères, J.-D., Picot, N., Moreau, T., & Raynal, M. (2017). CryoSat-2 SAR-mode over oceans: Processing methods, global assessment, and benefits. *IEEE Transactions on Geoscience and Remote Sensing*, *55*, 148–158. doi: 10.1109/TGRS.2016.2601958

Callahan, P. (2010, October). *Overview of TOPEX center of mass correction.* Ocean Surface Topography Science Team meeting, Lisbon. Retrieved from https://www.aviso.altimetry.fr/fileadmin/documents/OSTST/2010/oral/20_Wednesday/morning/Callahan.pdf

Carrère, L., Allain, D., Lyard, F., Faugère, Y., Baghi, R., Lachiver, J., ... Dibarboure, G. (2018, September). *Progress and challenges of the Dynamic Atmospheric Correction for altimetry over the last 25 years.* 25 years of progress in radar altimetry symposium. Retrieved from https://ostst.aviso.altimetry.fr/fileadmin/user_upload/TID_04_CARRERE.pdf

Carrère, L., Faugère, Y., & Ablain, M. (2016). Major improvement of altimetry sea level estimations using pressure-derived corrections based on ERA-Interim atmospheric reanalysis. *Ocean Science*, *12*, 825–842. doi: 10.5194/os-12-825-2016

Carrère, L., & Lyard, F. (2003). Modeling the barotropic response of the global ocean to atmospheric wind and pressure forcing – comparisons with observations. *Geophysical Research Letters*, *30*(6), 1275. doi: 10.1029/2002GL016473

Cartwright, D. E., & Edden, A. C. (1973). Corrected tables of tidal harmonics. *Geophysical Journal of the Royal Astronomical Society*, *33*, 253–264.

Cartwright, D. E., & Ray, R. D. (1991). Energetics of global ocean tides from Geosat altimetry. *Journal of Geophysical Research*, *96*, 16897–16912.

Cartwright, D. E., & Ray, R. D. (1994). On the radiational anomaly in the global ocean tide with reference to satellite altimetry. *Oceanologica Acta*, *17*, 453–459.

Desai, S. D., & Ray, R. D. (2014). Consideration of tidal variations in the geocenter for satellite altimeter observations of ocean tides. *Geophysical Research Letters*, *89*, 2454–2459. doi: 10.1002/2014GL059614

Desjonqueres, J.-D., Callihan, P. S., & Desai, S. D. (2023). *Topex/Poseidon GDR-F products handbook* (Reference No. JPL-D-73899). Pasadena: Jet Propulsion Laboratory. Retrieved from https://www.aviso.altimetry.fr/fileadmin/documents/data/tools/hdbk_tpx_grdf.pdf

Diaz-Argandoña, J., Ezcurra, A., Sáenz, J., Ibarra-Berastegi, G., & Errasti, I. (2016). Climatology and temporal evolution of the atmospheric semidiurnal tide in present-day reanalyses. *Journal of Geophysical Research: Atmospheres*, *121*, 4614–4626. doi: 10.1002/2015JD024513

Dobslaw, H., & Thomas, M. (2005). Atmospheric induced oceanic tides from ECMWF forecasts. *Geophysical Research Letters*, *32*. doi: 10.1029/2005GL022990

Goring, D. G., & Pyne, A. (2003). Observations of sea-level variability in Ross Sea, Antarctica. *New Zealand Journal of Marine and Freshwater Research*, *37*, 241–249.

Haigh, I. D., Marcos, M., Talke, S. A., Woodworth, P. L., Hunter, J. R., Hague, B. S., ... Thompson, P. (2022). GESLA version 3: A major update to the global higher-frequency sea-level dataset. *Geoscience Data Journal*, *00*, 00. doi: 10.1002/gdj3.174

Hart-Davis, M. G., Andersen, O. B., Ray, R. D., Zaron, E. D., Schwatke, C., Arildsen, R., ... Nielsen, K. (2024). Tides in complex coastal regions: Early case studies from wide-swath SWOT measurements. *Geophysical Research Letters*, *51*, e2024GL109983. doi: 10.1029/2024GL109983

Hart-Davis, M., Dettmering, D., & Seitz, F. (2022). *TICON-3: Tidal constants based on GESLA-3 sea-level records from 5,119 globally distributed tide gauges including gauge type information.* Deutsches Geodätisches Forschungsinstitut, München. (https://mediatum.ub.tum.de/doc/1693751/document.pdf)

Hart-Davis, M. G., Dettmering, D., Sulzbach, R., Thomas, M., Schwatke, C., & Seitz, F. (2021). Regional evaluation of minor tidal constituents for improved estimation of ocean tides. *Remote Sensing*, *13*, 3310. doi: 10.3390/rs13163310

Hart-Davis, M. G., Piccioni, G., Dettmering, D., Schwatke, C., Passaro, M., & Seitz, F. (2021). EOT20: a global ocean tide model from multi-mission satellite altimetry. *Earth System Science Data*, *13*, 3869–3884. doi: 10.5194/essd-13-3869-2021

Hersbach, H., et al. (2020). The ERA5 global reanalysis. *Quarterly Journal of the Royal Meteorological Society*, *146*, 1999–2049. doi: 10.1002/qj.3803

Idier, D., Bertin, X., Thompson, P., & Pickering, M. D. (2019). Interactions between mean sea level, tide, surge, waves and flooding: Mechanisms and contributions to sea level variations at the coast. *Surveys in Geophysics*, *40*, 1603–1630. doi: 10.1007/s10712-019-09549-5

King, M. A. (2006). Kinematic and static GPS techniques for estimating tidal displacements with application to Antarctica. *Journal of Geodynamics*, *41*, 77–86. doi: 10.1016/j.jog.2005.08.019

Kubitschek, D. G. (1997). *The anomalous acceleration and radiation force calculation for the TOPEX/Poseidon spacecraft* (PhD thesis). University of Colorado, Boulder.

Kubitschek, D. G., & Born, G. H. (2001). Modelling the anomalous acceleration and radiation pressure forces for the TOPEX/POSEIDON spacecraft. *Philosophical Transactions of the Royal Society*, *359*, 2191–2208. doi: 10.1098/rsta.2001.0882

Le Provost, C., Genco, M. L., Lyard, F., Vincent, P., & Canceil, P. (1994). Spectroscopy of the world ocean tides from a finite element hydrodynamic model. *Journal of Geophysical Research*, *99*, 24777–24797.

Leuliette, E. W., Scharroo, R., Smith, W. H. F., Lillibridge, J. L., & Miller, L. (2010, October). *An investigation into the source of the 59-day variations in Jason sea level.* Ocean Surface Topography Science Team meeting, Lisbon. Retrieved from `https://www.aviso.altimetry.fr/fileadmin/documents/OSTST/2010/oral/20_Wednesday/morning/Leuliette.pdf`

Lyard, F., Allain, D., Cancet, M., Carrère, L., & Picot, N. (2021). FES2014 global ocean tides atlas: design and performance. *Ocean Science*, *17*, 615–649. doi: 10.5194/os-17-615-2021

Lyard, F., Lefevre, F., Letellier, T., & Francis, O. (2006). Modelling the global ocean tides: modern insights from FES2004. *Ocean Dynamics*, *56*, 394–415. doi: 10.1007/s10236-006-0086-x

Munk, W. H., & Cartwright, D. E. (1966). Tidal spectroscopy and prediction. *Philosophical Transactions of the Royal Society*, *A259*, 533–581.

Munk, W. H., & MacDonald, G. J. F. (1960). *The Rotation of the Earth: A Geophysical Discussion*. Cambridge: Cambridge Univ. Press.

Naeije, M., & Bouffard, J. (2021). Long-term quality and stability assessment of CryoSat-2 ocean data. *Advances in Space Research*, *68*, 1194–1215. doi: 10.1016/j.asr.2019.08.039

Naeije, M., Schrama, E., & Scharroo, R. (2000). The radar altimeter database system project RADS. In *Igarss 2000. international geoscience and remote sensing symposium. taking the pulse of the planet: The role of remote sensing in managing the environment* (Vol. 2, pp. 487–490). IIIE. doi: 10.1109/IGARSS.2000.861605

Padman, L., Erofeeva, S. Y., & Fricker, H. A. (2008). Improving Antarctic tide models by assimilation of ICESat laser altimetry over ice shelves. *Geophysical Research Letters*, *35*, L22504. doi: 10.1029/2008GL035592

Piccioni, G., Dettmering, D., Bosch, W., & Seitz, F. (2019). TICON: Tidal constants based on GESLA sea-level records from globally located tide gauges. *Geoscience Data Journal*, *6*, 97–104. doi: 10.1002/gdj3.72

Ponte, R. M., & Ray, R. D. (2002). Atmospheric pressure corrections in geodesy and oceanography: a strategy for handling air tides. *Geophysical Research Letters*, *29*(24), 2153. doi: 10.1029/2002GL016340

Prandle, D., & Wolf, J. (1978). The interaction of surge and tide in the North Sea and River Thames. *Geophysical Journal of the Royal Astronomical Society*, *55*, 203–216.

Ray, R. D. (1999). *A global ocean tide model from Topex/Poseidon altimetry: GOT99.2* (NASA Tech. Memo. No. 209478). Greenbelt MD: Goddard Space Flight Center.

Ray, R. D. (2007). Propagation of the overtide M_4 through the deep Atlantic Ocean. *Geophysical Research Letters*, *34*, L21602. doi: 10.1029/2007GL031618

Ray, R. D. (2008). A preliminary tidal analysis of ICESat laser altimetry: Southern Ross Ice Shelf. *Geophysical Research Letters*, *35*, L02505. doi: 10.1029/2007GL032125

Ray, R. D. (2013). Precise comparisons of bottom-pressure and altimetric ocean tides. *Journal of Geophysical Research: Oceans*, *118*, 4570–4584. doi: 10.1002/jgrc.20336

Ray, R. D. (2017). On tidal inference in the diurnal band. *Journal of Atmospheric and Oceanic Technology*, *34*, 437–446. doi: 10.1175/JTECH-D-16-0142.1

Ray, R. D. (2020). First global observations of third-degree ocean tides. *Science Advances*, *6*, eabd4744. doi: 10.1126/sciadv.abd4744

Ray, R. D., & Erofeeva, S. Y. (2014). Long-period tidal variations in the length of day. *Journal of Geophysical Research: Solid Earth*, *119*, 1498–1509. doi: 10.1002/2013JB010830

Ray, R. D., Larson, K. M., & Haines, B. J. (2021). New determinations of tides on the north-western Ross Ice Shelf. *Antarctic Science*, *33*, 89–102. doi: 10.1017/S0954102020000498

Ray, R. D., & Schindelegger, M. (2025). Trends in the M_2 ocean tide observed by satellite altimetry in the presence of systematic errors. *Journal of Geodesy*, *99*, 11. doi: 10.1007/s00190-025-01935-9

Sánchez-Román, A., Pujol, M. I., Faugère, Y., & Pascual, A. (2023). DUACS DT2021 reprocessed altimetry improves sea level retrieval in the coastal band of the European seas. *Ocean Science*, *19*, 793–809. doi: 10.5194/os-19-793-2023

Scharroo, R. (2014). *RADS RDSAR Algorithm Theoretical Basis Document vers. 0.3* (CP4O ESA Project Rep.) Altimetrics. Retrieved from `http://www.satoc.eu/projects/CP4O/docs/tud_rdsar_atbd.pdf`

Scharroo, R. (2024). *RADS data manual, version 4.6.3* (Tech. Rep.). EUMETSAT & Tech. Univ. Delft.

Scharroo, R., Leuliette, E. W., Lillibridge, J. L., Byrne, D., Naeije, M. C., & Mitchum, G. T. (2013). RADS: Consistent multi-mission products. In *Proc. Symposium on 20 Years of Progress in Radar Altimetry.* (ESA Spec. Publ. SP-710)

Schrama, E., Scharroo, R., & Naeije, M. (2000). *Radar altimeter database system (RADS): Towards a generic multi-satellite altimeter database system* (DEOS Report). Delft: Delft Inst. Earth-Oriented Space Research.

Schrama, E. J. O., & Ray, R. D. (1994). A preliminary tidal analysis of TOPEX/Poseidon altimetry. *Journal of Geophysical Research*, *99*, 24799–24808.

Shihora, L., Balidakis, K., Dill, R., Dahle, C., Ghobadi-Far, K., Bonin, J., & Dobslaw, H. (2022). Non-tidal background modeling for satellite gravimetry based on operational ECMWF and ERA5 reanalysis data: AOD1B RL07. *Journal of Geophysical Research: Solid Earth*, *127*, e2022JB024360. doi: 10.1029/2022JB024360

Stammer, D., et al. (2014). Accuracy assessment of global barotropic ocean tide models. *Reviews of Geophysics*, *52*, 243–282. doi: 10.1002/2014RG000450

Szpilka, C., Dresback, K., Kolar, R., Feyen, J., & Wang, J. (2016). Improvements for the Western North Atlantic, Caribbean and Gulf of Mexico ADCIRC tidal database EC2015. *Journal of Marine Science and Engineering*, *4*, 72. doi: 10.3390/jmse4040072

Szpilka, C., Dresback, K., Kolar, R., & Massey, T. C. (2018). Improvements for the Eastern North Pacific ADCIRC tidal database ENP2015. *Journal of Marine Science and Engineering*, *6*, 131. doi: 10.3390/jmse6040131

Wahr, J. M. (1981). Body tides on an elliptical, rotating, elastic and oceanless earth. *Geophysical Journal of the Royal Astronomical Society*, *64*, 677–704.

Williams, R. T., & Robinson, E. S. (1980). The ocean tide in the southern Ross Sea. *Journal of Geophysical Research*, *85*, 6689–6696.

Woodworth, P. L., Hunter, J. R., Marcos, M., Caldwell, P., Menéndez, M., & Haigh, I. (2017). Towards a global higher-frequency sea level dataset. *Geoscience Data Journal*, *3*, 50–59. doi: 10.1002/gdj3.42

Zaron, E. D. (2018). Ocean and ice shelf tides from CryoSat-2 altimetry. *Journal of Physical Oceanography*, *48*(4), 975–993. doi: 10.1175/JPO-D-17-0247.1

Zaron, E. D., & Elipot, S. (2024). Estimates of baroclinic tidal sea level and currents from Lagrangian drifters and satellite altimetry. *Journal of Atmospheric and Oceanic Technology*, *41*, 781–802. doi: 10.1175/JTECH-D-23-0159.1

Zaron, E. D., & Ray, R. D. (2018). Aliased tidal variability in mesoscale sea level anomaly maps. *Journal of Atmospheric and Oceanic Technology*, *35*, 2421–2435. doi: 10.1175/JTECH-D-18-0089.1

Zawadzki, L., Ablain, M., Carrere, L., Ray, R. D., Zelensky, N. P., Lyard, F., . . . Picot, N. (2018). Investigating the 59-day error signal in the mean sea level derived from Topex/Poseidon, Jason-1, and Jason-2 data with FES and GOT ocean tide models. *IEEE Transactions on Geoscience and Remote Sensing*, *56*, 3244–3255. doi: 10.1109/TGRS.2018.2796630